





Final Report

Project Title: A Study into the Effectiveness of Crystallization Process in Purification of Active Pharmaceutical Ingredients

By Dr.Lek Wantha

Contract No. MRG5680123

Final Report

Project Title: A Study into the Effectiveness of
Crystallization Process in Purification of Active
Pharmaceutical Ingredients

Dr.Lek Wantha Burapha University

This project granted by the Thailand Research Fund

บทคัดย่อ

รหัสโครงการ : MRG5680123

ชื่อโครงการ: การศึกษาถึงประสิทธิภาพของกระบวนการตกผลึกในการทำบริสุทธิ์

ตัวยาสำคัญ

ชื่อนักวิจัย: ดร.เล็ก วันทา มหาวิทยาลัยบูรพา

E-mail Address: lekw@eng.buu.ac.th

ระยะเวลาโครงการ : 3 มิถุหายห 2556 ถึง 2 มิถุหายห 2558

บทคัดย่อ

สารตัวยาสำคัญที่ใช้ในการทดลองในงานวิจัยนี้ คือ แอลฮีสทิดีน พหุสันฐานของแอลฮีส ทิดีนที่ค้นพบตอนนี้มีอยู่สองรูปแบบ คือ รูปแบบ A ที่เสถียร และรูปแบบ B ที่ไม่เสถียร โดยทั่วไปการเกิดขึ้นของพหุสันฐานแต่ละสันฐานจะขึ้นอยู่กับอุณหพลศาสตร์ จลนศาสตร์ของ การตกผลึก จลนศาสตร์ของการละลาย และจลนศาสตร์ของการเปลี่ยนรูปผลึก งานวิจัยนี้มี วัตถุประสงค์เพื่อศึกษา ทำความเข้าใจและวิเคราะห์ถึงลักษณะของจลนศาสตร์ของการตกผลึก และการละลายของพหุสันฐานทั้งสอง นอกจากนี้ยังศึกษาเกี่ยวกับพฤติกรรมการตกผลึกของ พหุสันฐานทั้งสองในสารละลายน้ำและเอทานอลด้วย

ทำการทดลองวัดอัตราการโตของผลึกรูปแบบ A และการละลายของผลึกรูปแบบ B ใน สารละลายน้ำที่อุณหภูมิ 10, 25, และ 40 °C ด้วยวิธี desupersaturation สำหรับวัดอัตราการโต และวิธี deundersaturation สำหรับวัดอัตรการละลาย จากการทดลองพบว่าทั้งอัตราการโตของ ผลึกรูปแบบ A และการละลายของผลึกรูปแบบ B มีค่าเพิ่มขึ้นเมื่ออุณหภูมิเพิ่มขึ้น ที่อุณหภูมิทั้ง สามค่าพบว่าอัตราการละลายของผลึกรูปแบบ B มีค่าสูงกว่าอัตราการโตของผลึกรูปแบบ A แสดงให้เห็นว่ากระบวนการเปลี่ยนรูปผลึกจากรูปแบบ B ที่ไม่เสถียรไปเป็นรูปแบบ A ที่เสถียร โดยอาศัยสารละลายเป็นสื่อกลางจะถูกควบคุมโดยกระบวนการโตของผลึกรูปแบบ A ที่เสถียร

การศึกษากลไกการเกิดและการโตของผลึกรูปแบบ B ในสารละลายน้ำและเอทานอลถูก ศึกษาโดยวิธีการวัดเวลาเหนี่ยวนำ โดยทำการศึกษาที่ความเข้มข้นเกิดจุดอื่มตัวค่าต่าง ๆ นอกจากนี้ยังได้ศึกษาผลึกที่เกิดขึ้นในช่วงเริ่มต้นการตกผลึกจากสารละลายน้ำและเอทานอลว่า ผลึกที่ได้นั้นเป็นผลึกรูปแบบใด เวลาเหนียวนำที่วัดได้ถูกนำไปประมาณค่ากับสมการทาง คณิตศาสตร์ของแบบจำลองกลไกการเกิดและการโตของผลึกของสองแบบจำลอง คือ แบบจำลอง mononuclear และ polynuclear จากการศึกษาพบว่ากลไกการเกิดเป็นแบบจำลอง polynuclear และกลไกการโตเป็นแบบจำลอง two-dimensional nucleation-mediated growth และผลึกที่ได้ในช่วงต้นของการตกผลึกจะขึ้นกับสัดส่วนโดยปริมาตรของเอทานอลที่เติมลงไป กล่าวคือ จะเป็นผลึกรูปแบบ B ที่ไม่เสถียรเมื่อสัดส่วนโดยปริมาตรของเอทานอลมีค่าสูงๆ และ จะเป็นผลึกรูปแบบ A ผสมกับ B เมื่อสัดส่วนโดยปริมาตรของเอทานอลมีค่าต่ำ ๆ

คำหลัก: การละลายของผลึก การโตของผลึก การเกิดของผลึก ภาวะพหุสัณฐาน ผลึกรูปแบบ A ที่เสถียรของแอลฮีสทิดีน ผลึกรูปแบบ B ที่ไม่เสถียรของแอลฮีสทิดีน **Abstract**

Project Code: MRG5680123

Project Title: A Study into the Effectiveness of Crystallization Process in

Purification of Active Pharmaceutical Ingredients

Investigator: Dr.Lek Wantha Burapha University

E-mail Address : lekw@eng.buu.ac.th

Project Period: 3 June 2013 to 2 June 2015

Abstract

In this work, the active pharmaceutical ingredient (API), L-histidine (L-his), was

used to be the model substance. There are two known polymorphic forms of L-his, the

stable polymorph, A, and the metstable (unstable) polymorph, B. The formation of

polymorphs is usually determined by thermodynamics, crystallization and dissolution

kinetics, and transformation kinetics. This research aims to understand and predict the

crystallization and dissolution kinetics of these polymorphs. The behavior of the

crystallization in aqueous and water-ethanol solutions (anti-solvent crystallization) was

also studied.

Experimental measurements of the growth rate of form A and the dissolution

rate of form B in aqueous solution were performed at 10, 25, and 40 °C. The growth

and dissolution kinetics were measured using desupersaturation and deundersaturation

techniques, respectively. Both the growth and dissolution rates increase with increasing

temperature. At all temperatures studied, the dissolution rate of form B is faster than the

growth rate of form A, indicating that the solution-mediated transformation (SMT) of the

polymorphs of L-his is likely to be controlled by the growth rate of form A.

The nucleation and growth mechanisms of form B in a water-ethanol system

were determined based on the induction time measurements. The induction times were

experimentally determined at different supersaturations. The experimental results of

induction time were correlated using the models of mononuclear and polynuclear mechanisms. The results showed that the primary nucleation mechanism of form B is identified as a polynuclear mechanism, and the growth mechanism is identified as two-dimensional nucleation-mediated growth. Moreover, the formation of the polymorphs from crystallization in water-ethanol solutions as a function of supersaturation and ethanol volume fraction was studied. The results showed that form B was obtained initially at higher ethanol volume fraction and supersaturation. A mixture of forms A and B was obtained at lower ethanol volume fraction and supersaturation.

Keywords: Crystal Dissolution, Crystal Growth, Crystal Nucleation, Polymorphism,

A polymorph of L-histidine, B Polymorph of L-histidine

1. Introduction to the Research Problem and Its Significance

Recently, the solid forms of drug are very important in pharmaceutical industries. These forms of active pharmaceutical ingredient (API) are used more frequently than other dosage forms. This is since the liquid forms metabolize quickly in the bloodstream requiring increased dosage as part of the treatment, while solid forms provide a longer therapeutic effect with a reduced dosage (Suarez et al., 2001) which provide an easier management. The prolonged action of a solid form depends on its physical state because crystals in the crystalline form have longer time of action than amorphous crystals.

The key problem in production of the solid forms of APIs is that many APIs occur as several crystal polymorphs (the same chemical in a different crystal structure) and/or solvates and psuedopolymorphs (the same chemical, but with a water or solvent molecule in the crystal structure). Polymorphs and solvates can have different mechanical, thermal, physical, and chemical properties. Because of the different properties of polymorphs, it is advantageous to choose the proper polymorph for the desired application. Therefore, in the crystallization processes involving polymorphs, the formation of the desired polymorph has to be controlled and such a process should be robust and reproducible. In many cases, if both polymorphs crystallize at approximately similar rates, the two polymorphs may crystallize simultaneously from the solution, also called concomitant polymorphism (Bernstein et al., 1999), even with the unstable polymorph predominating, and this is sometimes not acceptable from the point of view of obtaining polymorphically pure compounds suitable for sale, particular in the food and other material products. On the other hand, in the field of pharmaceuticals, metastable polymorphs may be more desirable than stable polymorphs. Methods of inhibiting particular polymorphs or solvates are necessary to create polymorphically pure compounds. This study aims to make conclusions about methods to produce a polymorphically pure API compounds by crystallization. The crystallization and dissolution kinetics were studied to be the data for supporting this conclusion. L-histidine

(L-his) was the model substance of API compound. L-his crystal has previously been shown to exhibit polymorphism and exists in the solid phase as a stable polymorph A and a metastable polymorph B (Kitamura, 1993; Roelands et al., 2006).

2. Theory and Literature Review

2.1 Polymorphism

Polymorphism is the ability of a solid compound to exist in more than one crystalline form (Grant, 1999). These crystalline forms, although containing the same molecules, result from a different ordered arrangement of molecules within the crystalline lattice. Solvates in the contrary, incorporate molecules of one or more solvents. Polymorphs and solvates can have different mechanical, thermal, physical, and chemical properties, such as compressibility, melting point, crystal habit, color, density, dissolution rate, solubility, bio-availability or chemical reactivity (Yu, Reutzel-Edens et al., 2000; Yu, Chew et al., 2007). In recognition of a different need, all industries related to pure or formulated solids, especially the pharmaceutical industry know about the importance of polymorph or solvate monitoring and control (including formation, prediction, transformation, and stability) (Mangin et al., 2009; Yu, Chew et al., 2007). Later require a deep understanding of the kinetics (crystallization, dissolution, and transformation kinetics) and thermodynamics of the polymorphic or solvate system.

Polymorphism and solvates are of great importance phenomenon, particularly in the pharmaceutical industry as different polymorphs and solvates can exhibit different properties with great influence on the bio-availability, stability, filtration, drying, grinding, and tableting properties of the drug substance (Chen et al., 2011; Parmar et al., 2007). Generally, the thermodynamically stable polymorph or solvate is more desirable commercial dosage form than metastable polymorph or solvate. This indicates that the unknown polymorphs or solvates that formed during production or uncontrolled transformation is highly undesirable. However, e.g. in the case of API which usually has low solubility in water, the stable polymorph which also shows the lowest solubility,

might have an insufficient bio-availability (Ulrich and Frohberg, 2012). Therefore, to improve a certain properties such as a higher bio-availability the metastable polymorphs or solvates, which shows higher solubility, have to be developed (Capes and Cameron, 2006; Mangin et al., 2009). The example of the solubility of the polymorphic compound that follows this system is shown in Figure 1. This figure is the solubility data of α -form (metastable form) and β -form (stable form) of L-glutamic acid. L-glutamic acid is one example of a monotropic system. The β -form is stable relative to the others at all temperatures below the melting point; the polymorphs are not interconvertible, and the solubility is always lower than that of the metastable α -form. Another example of the solubility data is shown in Figure 2. This is the data for L-phenylalanine which is one example of an enantiotropic system. The stable polymorphic form depends on the temperature and pressure of the system, there is a reversible transition point below the melting points of the polymorphs where the relative thermodynamic stabilities change. Moreover, the metastable form may exist for a long time and the presence of the stable form results in mediated phase transformation.

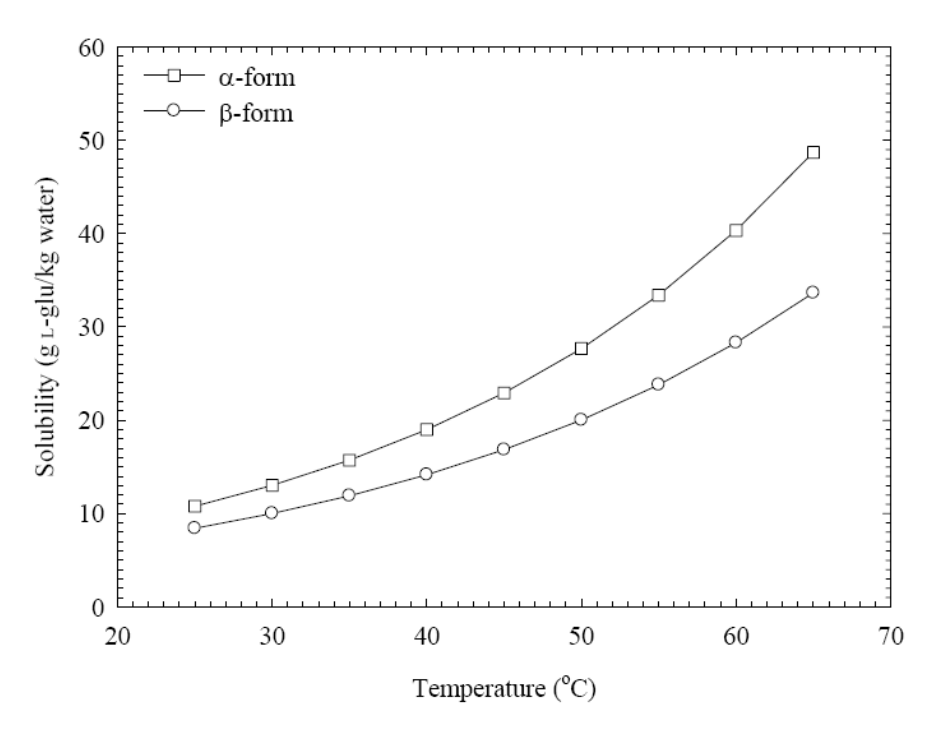


Figure 1. Solubility curves for two polymorphic forms of L-glutamic acid.

(Kee et al., 2009)

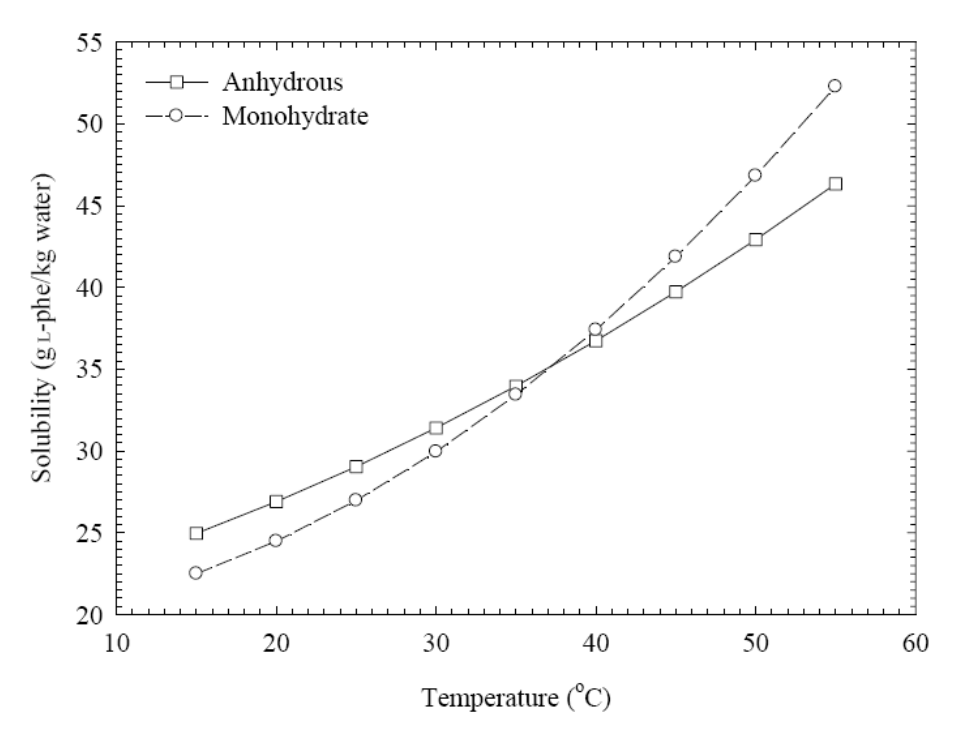


Figure 2. Solubility curves of L-phenylalanine polymorph. (Mohan et al., 2001)

2.2 Polymorphic Crystallization

Crystallization is a phase change in which a crystalline product is obtained from solution. A solution is a homogeneous single phase that is formed by the mixing of two or more species. Solutions are normally liquid, however, solutions may include solids and even gases. Typically, for the current work, the term solution means a liquid solution consisting of a solvent, which is a liquid as a pure species at the conditions, (*T*, *P*), of the solution, and a solute, which is a solid as a pure species at the conditions of interest. The term melt means a material that is solid at ambient conditions and is heated until it becomes a molten liquid. Melts may be pure material or they may be mixtures of materials.

Crystallization is a separation and purification process used to produce a wide variety of materials in the fine chemical, food, and pharmaceutical industries. In the pharmaceutical industry crystallization is used as a separation and purification processes for intermediates and often serves as the final step in the manufacture of APIs (Chen et al., 2011). Several crystallization methods are known to crystallize a less

stable (metastable) polymorph or solvate of a drug, which is the form most suitable in the field of pharmaceuticals (Capes and Cameron, 2006; Chen et al., 2011). These include high pressure crystallization (Griesser et a., 1997), spray drying (Beckmann and Otto, 1996), crystallization from a melt or a quenched amorphous state (Stowell et al., 2002), crystallization from solution (Bobrovs et al., 2014; Lu et al., 2007). However, they have been found to be difficult to control precisely to avoid the formation of more than one polymorph (Capes and Cameron, 2006; Zencirci et al., 2009).

It is necessary to prepare the appropriate polymorph for the desired application. Therefore, the formation of the desired polymorph has to be controlled in polymorphic crystallization and such a process should be robust and reproducible. Usually, the formation of the polymorph is determined by thermodynamics, crystallization and dissolution kinetics, and transformation kinetics. Thermodynamics are used to identify whether the crystal phase is the stable or metastable polymorph. Kinetics are used to determine how fast these crystal phases can be crystallized at a certain driving force. Polymorphic crystallizations consist of the competitive nucleation and crystal growth of the polymorphs and the transformation from the metastable polymorph to the stable polymorph, usually via a solution-mediated transformation (SMT) mechanism, particularly in crystallization from solution. This consists of the nucleation and crystal growth of the stable polymorph and the dissolution of the metastable polymorph (Jiang et al., 2010; Mangin et al., 2009; O'Mahony et al., 2012; Wantha and Flood, 2013a). Therefore, the mechanism and kinetics of each elementary step in the crystallization process needs to be understood to predict and control the formation of the appropriate polymorph.

Accurate modeling of the SMT can be performed by creating separate models of each of the mechanisms involved and combining these models within the framework of the population balance equation (PBE) (Févotte et al., 2007; Wantha and Flood, 2013b). This is a two-step method. Firstly, the rates of the crystallization processes (nucleation and growth) and the rate of dissolution of each polymorph are obtained through specific

experiments. Secondly, the rates of crystallization and dissolution of each polymorph are then combined in the PBE in order to estimate the time of the transformation, polymorphic fraction profile, concentration profile, etc., which can then be compared with the results from a SMT experiment.

2.3 Crystal Nucleation and Growth

Crystallization from solution is usually the result of two processes; crystal nucleation and crystal growth. Nucleation involves a process of fluctuation of the size of nanoscopically small molecular clusters potentially creating nuclei of the new crystalline phase. This leads to the formation of new crystals in the liquid solution. Nucleation is classified into primary and second nucleation (Figure 3). Primary nucleation is the birth of new crystals from a liquid or solution that contains no crystalline material of the nucleating solute, and is divided into homogeneous primary nucleation and heterogeneous primary nucleation. In homogeneous primary nucleation there are no external nucleation sites available (as could be caused by the walls of the vessel, dust particles, crystals or solids of other solutes, etc.), and the nuclei are formed by statistical fluctuations of solute entities that cluster together (Kramer and van Rosmalen, 2009). Heterogeneous primary nucleation occurs when the presence of such foreign surfaces assists in obtaining primary nuclei. Secondary nucleation is the formation of new nuclei which occurs due to the presence of crystals of the crystallizing material that are already present in the solution. Secondary nucleation is far more significant than primary nucleation in most industrial crystallization units because the vessel is run continuously having solute crystals inside.

Up until now there have been numerous techniques for determination of the nucleation rate for the crystallization process have been proposed in the literature, for example, methods using combined particle (crystal) counting and process time measurements (Lindenberg and Mazzotti, 2011; Wantha and Flood, 2012), mixed-suspension mixed-product removal (MSMPR) experiments in combination with particle

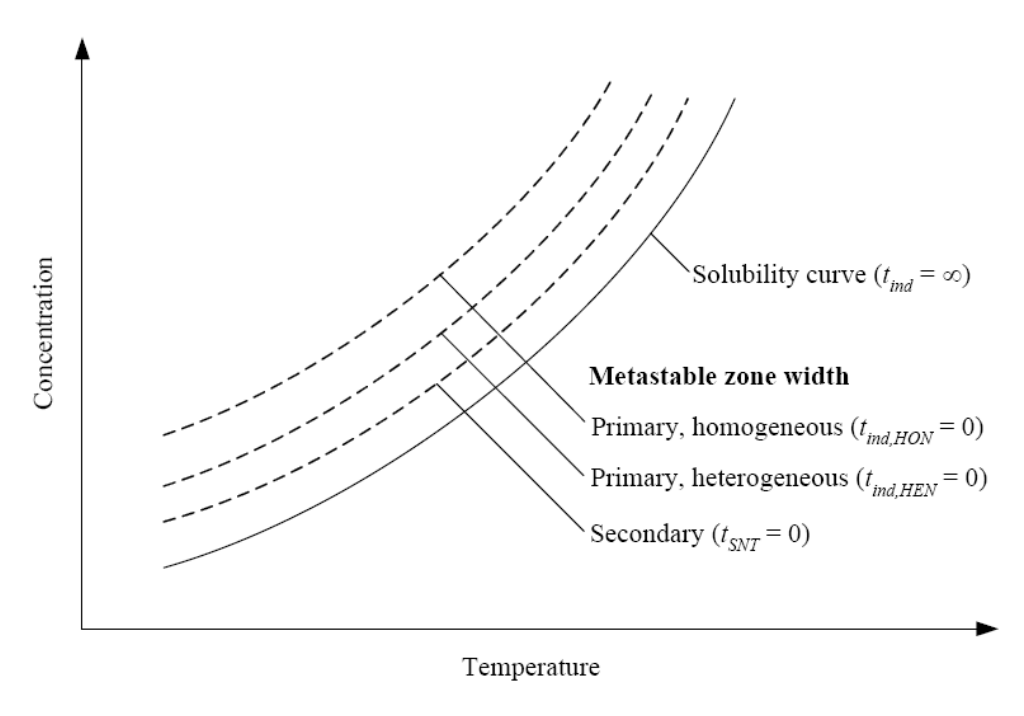


Figure 3. Instantaneous metastable zone widths for different nucleation mechanisms. The variables t_{SNT} , $t_{ind,HEN}$, and $t_{ind,HON}$, are the induction time for secondary nucleation, heterogeneous, and homogeneous nucleation, respectively. (Wantha, 2011)

size distribution (PSD) measurements (Garside et al., 2002; Mersmann, 2001), induction time measurements (Lindenberg and Mazzotti, 2009; Teychené and Biscans, 2008; Zhi et al., 2011), and metastable zone experiments (Mitchell and Frawley, 2010; Nagy et al., 2008). The method that has been widely used is the method of induction time measurement (Lindenberg and Mazzotti, 2009; Teychené and Biscans, 2008; Zhi et al., 2011). In refs. (Teychené and Biscans, 2008; Zhi et al., 2011), the theoretical expressions have been used to show the dependence of the induction time on the supersaturation for different crystal growth mechanisms. These expressions have been shown to be correct in identifying the nucleation and growth mechanisms. Therefore, in this research the nucleation and growth mechanisms were determined by induction time measurements.

The classical nucleation theory (CNT) of primary nucleation has been described as follows by Kuldipkumar *et al.* (2007). The rate of primary nucleation can be described according to the following equation:

$$J = A \exp\left(\frac{-4f_s^3 \gamma^3 v^2}{27f_v^2 \kappa^3 T^3 (\ln S)^2}\right)$$
 (1)

where A is the pre-exponential factor, γ is the interfacial free energy between crystal and solution, ν is the molecular volume of the crystal, κ is the Boltzmann constant, T is the absolute temperature, S is the supersaturation ($S = C/C^*$), f_s is the surface shape factor, and f_{ν} is the volume shape factor.

For a mononuclear nucleation mechanism, Mullin (2001) suggested that the induction time period t_{ind} is inversely proportional to the nucleation rate ($t_{ind} = 1/JV$), and then Eq. (1) can be rewritten as

$$\ln t_{ind} = A_m + \frac{B}{(\ln S)^2} \tag{2}$$

when

$$A_m = \ln \frac{1}{AV} \tag{3}$$

$$B = \frac{4f_s^3 \gamma^3 v^2}{27f_v^2 \kappa^3 T^3} \tag{4}$$

where V is the volume of the system. A plot of $\ln(t_{ind})$ against $1/(\ln S)^2$ results a straight line of slope B, and intercept of axis y of A_m . The different slopes suggest that the homogeneous (at high supersaturation) and heterogeneous (at low supersaturation) nucleation mechanisms may exist (Mullin, 2001).

Eq. (2) is valid when the induction time is dominated by the time required for the critical nuclei formation; that is, the nucleation is due to a mononuclear nucleation mechanism (Zhi et al., 2011). However, Eq. (2) will be invalid if the induction time is dominated by the time required to grow the nucleus to be a detectable size (Zhi et al.,

2011). Therefore, the polynuclear mechanism should be adopted to characterize the nucleation.

The induction time for the formation of a new phase by the polynuclear mechanism is usually expressed as (Kuldipkumar et al., 2007):

$$t_{ind} = \left[\frac{\alpha}{a_n J G^{n-1}}\right]^{1/n} \tag{5}$$

where α is the volume fraction of the detected new phase, G is the growth rate of nucleus, a_n is the shape factor, and n=mb+1, where m refers to the dimensionality of growth, and b=0.5 or 1 denotes that the crystal growth is controlled by volume diffusion or by surface integration process, respectively. Because B polymorph of L-his is a plate crystal (Kitamura, 1993), a two-dimensional growth (m=2) can be assumed. Because growth of the L-his crystal is controlled by surface integration process (Wantha and Flood, 2015), b=1.

For the polynuclear nucleation mechanism, the pre-exponential factor in Eq. (1) depends on the supersaturation (Zettlemoyer, 1969). Therefore, the steady-state nucleation rate is written as

$$J = K_J S \exp\left(\frac{-B}{\left(\ln S\right)^2}\right) \tag{6}$$

where K_J is the nucleation rate constant.

The general growth kinetics can be expressed as a function of supersaturation by the power-law model (Mersmann, 2001; Mullin, 2001)

$$G = K_G (S - 1)^g = K_G \sigma_G^g \tag{7}$$

where K_G is growth rate constant, g is the growth rate order and indicates the growth mechanism. In general, a growth rate order of g=1 indicates that mass transfer becomes a rate-controlling mechanism, and a growth rate order between 1 and 2 indicates that the surface integration step is rate-controlling and represents the "birth and spread" growth mechanism, while g>2 represents a spiral growth mechanism. Substituting Eqs. (6) and (7) into Eq. (5), and taking the logarithm of the induction time (with m=2 and b=1), the following relationship can be obtained:

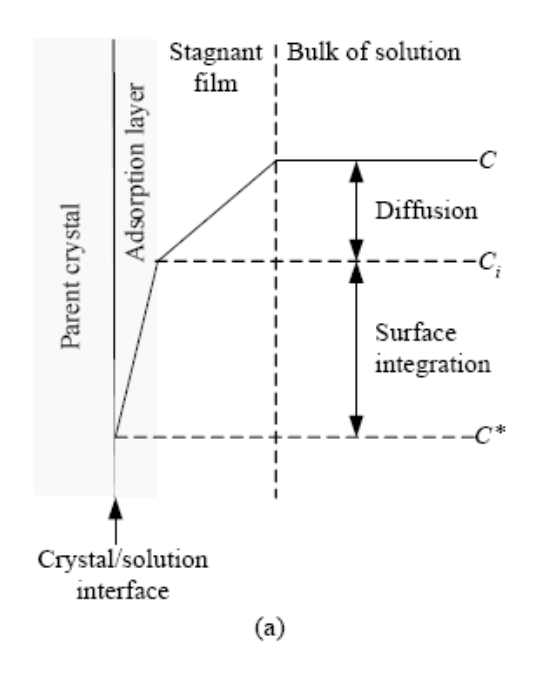
$$\ln t_{ind} = \ln A_P - \frac{2g}{3} \ln(S - 1) - \frac{1}{3} \ln S + \frac{B}{3 \ln^2 S}$$
 (8)

when

$$A_P = \left(\frac{\alpha}{a_n K_J K_G^2}\right)^{1/3} \tag{9}$$

The parameters of A_P , B, and g can be obtained by correlating the induction time with the supersaturation. The nucleation and growth mechanisms can be identified by comparing the coefficient of determination R^2 or values of g (Eq. (8)).

Crystal growth from solution is a two-step process (Randolph and Larson, 1988) (see Figure 4). The first step (mass transfer by diffusion or convection) involves the transfer of molecules from the bulk solution to the crystal surface. The second step concerns the insertion of the molecules into the crystal surface - a reaction step. The growth rate depends on the level of driving force for crystal growth which is the supersaturation. The dissolution process is usually considered to be controlled by the mass transfer of solute molecules from the crystal surface to the bulk, however it may also involve a reaction step. The dissolution rate depends on the level of driving force for dissolution which is the undersaturation. Crystal growth rate data of industrial crystallization processes are usually correlated empirically with supersaturation using a power-law model of the form as shown in Eq. (7).



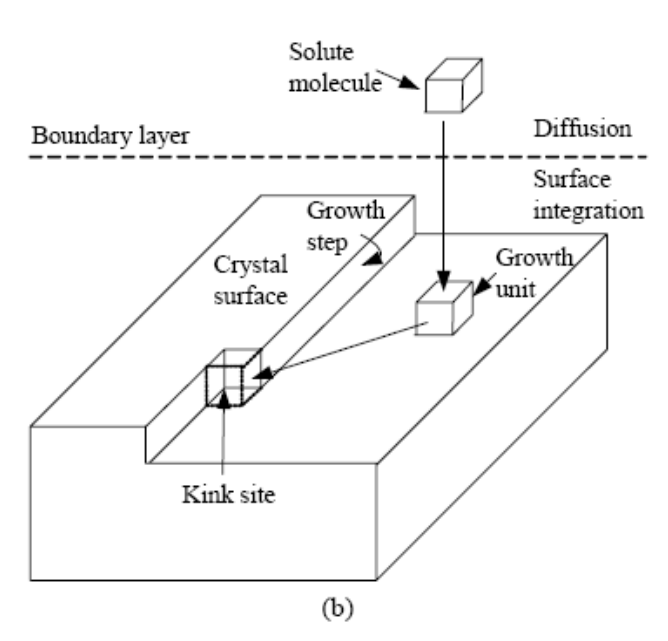


Figure 4. The model representation of the concentration driving force (a), and the two-step crystal growth process (b). (Wantha, 2011)

There are at least two main groups of techniques used to measure crystal growth rate. The first group is the single crystal growth methods, where the growth kinetics of different crystal faces are usually determined by optical or atomic force microscopy (Kitamura and Ishizu, 2000; Pantaraks and Flood, 2005). The second group is the methods involving growth in a multiparticle system (Kitamura et al., 1994; Srisanga et al., 2006). These techniques usually involve measuring the change in the mass

or size of a group of crystals at a fixed temperature and supersaturation. When a large number of crystals are analyzed to obtain an accurate mean crystal growth rate and the extent of growth rate dispersion the first technique may be more time consuming than the second technique. The desupersaturation experiment is another technique which is based on measuring the change of the particle size distributions (PSDs) and solute concentrations with time in a seeded isothermal batch experiment (Garside et al., 2002; Schöll et al., 2007; Wantha and Flood, 2011). The advantage of this method is that a large set of growth data can be obtained from a single experiment. The dissolution rate can be measured using the same method as the growth rate, where the size of a seed crystal (or crystals) increases with time during the growth experiment, while the size of a seed crystal (or crystals) decreases with time during the dissolution experiment (Gougazeh et al., 2009; Gutjahr et al., 1996; Wantha and Flood, 2013b). In this research, the growth and dissolution rates were measured using the desupersaturation and deundersaturation experiments, respectively.

2.4 Factor Effect on Polymorphic Crystallization

In many situations, the isolation of a metastable polymorph before it undergoes a solvent-mediated phase transformation to the more stable form is difficult and challenging (Wang et al., 2000). Therefore, several studies were investigated the use of additives (Davey et al., 1997; Gu et al., 2002) and substrates (Mitchell et al., 2001; Bonafede and Ward, 1995) to either encourage the preferential nucleation of one polymorph or to disrupt the crystal growth of the other form. However, the limited success of these methods is due to they do not take into account kinetic factors that are likely to play a dominant role during crystallization. As a consequence, to take advantage of the excellent properties of a metastable polymorph or solvate a kinetic stabilization by inhibiting the formation of a more stable polymorph or solvate is required (Gu et al., 2002).

The advanced methods to obtain desired metastable polymorphs or solvates are the use of external field or surface templating (Ulrich and Frohberg, 2012). The selective nucleation of a desired polymorph can be achieved by controlling the supersaturation and nucleation temperature, and choice of solvent or use of additives (Lu et al., 2010; Prashad et al., 2010). Another technique for selective nucleation is seeding experiments with great care by ensuring the absence of the stable polymorph nuclei while the nucleation of the metastable polymorph or solvate (Beckmann, 2000).

The other influential factors are supersaturation (Kitamura and Nakamura, 2002), stirring rate (Cashell et al., 2004), mixing rate of reactant solutions (in the case of reactive crystallization) (Kitamura et al., 2002), addition rate (Kim et al., 2003), and solvents (Bobrovs et al., 2014; Kitamura and Nakamura, 2002). In this work the effect of solvent was studied.

2.5 L-Histidine

Histidine (see Figure 5) is one of the essential amino acids. It is produced for use in a variety of products including as a food additive, an active pharmaceutical ingredient, in animal feed, and as a precursor for other chemicals. L-histidine (L-his) crystal has been known to have two polymorphs, form A and form B (Kitamura, 1993; Roelands et al., 2006). The crystal structure of form A and form B of L-his is shown in Figure 6. The molecular conformation is quite similar. Experimentally it is determined that form A is the stable form, and form B is the metastable (unstable) form. Form A is produced from the completed transformation of form B into form A in aqueous solution, and form B is produced from anti-solvent crystallization, where water is used as the solvent and ethanol is the anti-solvent (Kitamura, 1993; Roelands et al., 2006). The polymorphic transformation between form B and form A is particularly significant to the processing of histidine.

Histidine

Figure 5. Chemical structure of Histidine

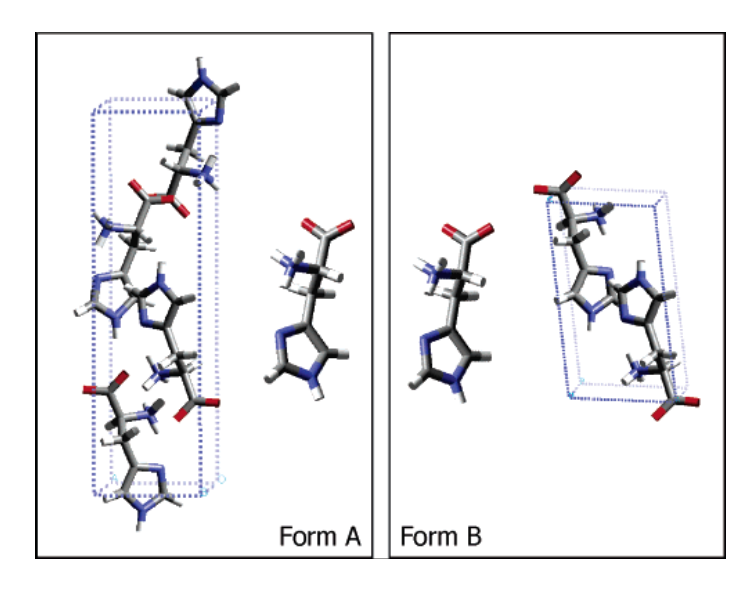


Figure 6. The crystal structure of form A and form B of L-histidine.

(Roelands et al., 2006)

3. Research Objectives

The objective of this reserch is to study and characterize the crystallization processes of the polymorphs of L-his in aqueous solution and water-ethanol solution. This includes measurement and analysis of the solid properties of each polymorph, measurement and analysis of the nucleation, growth, and dissolution kinetics of each polymorph. The effects of temperature, supersaturation (or undersaturation for dissolution), and solvent on these kinetics are studied.

4. Experimental Methods

4.1 Materials

Pure powder of L-his powder (>99%, Sigma-Aldrich), and ethanol (>99%, Carlo Erba Reagent) were used without further purification. Water used in the experiment was deionized water.

4.2 Preparation of Polymorphs A and B

The pure form of each polymorph was prepared by the following methods. Form B crystals were crystallized from an anti-solvent crystallization at room temperature as described elsewhere (Kitamura, 1993; Roelands et al., 2006). Previous studies have suggested using mixtures of water and ethanol (at greater than 40 percent volume ethanol) to produce from B. In this research, a saturated aqueous solution of L-his was prepared and from B crystallized by adding a volume of ethanol that was two times the volume of the original saturated solution. Form A crystals were obtained when the transformation from form B to form A was completed in aqueous solution at room temperature, as described elsewhere (Kitamura, 1993; Roelands et al., 2006). Pure crystal polymorphs of each form were also characterized by X-ray powder diffractometry (XRPD) and optical microscopy. Photomicrographs of crystals of form A and form B are shown in Figure 7. The shape of form A crystal is rod-like. The shape of form B crystal is plate-like. The characteristic peaks of XRPD of form A and B are shown in Figure 8. The XRPD patterns of pure forms A and B show some distinct differences.

The seed crystals of the pure form A were obtained by collecting sieved crystals in the size range of 125–250 μm . The crystal seed of the pure form B were obtained by collecting sieved crystals in the size ranges of 250–355 μm . The seed of form B were prepared at a larger size since the dissolution rate experiments involve a decrease in size of the seed crystals, and the decrease in size is relatively rapid; thus the dissolution experiments require large seed crystals to obtain reproducible results.

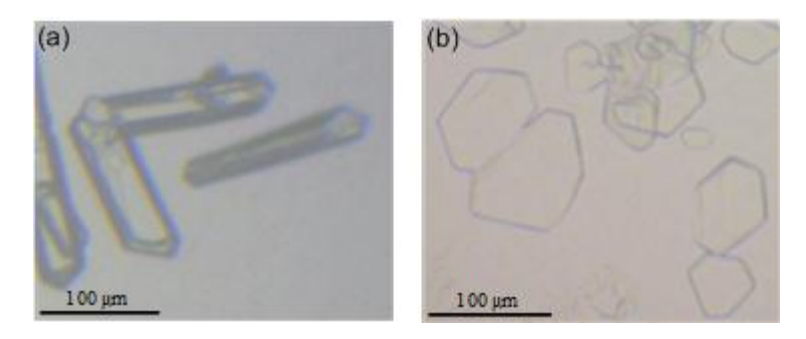


Figure 7. Photomicrographs of product crystals: obtained from the completed transformation of form B into form A in aqueous solution at 25 °C (a), obtained from water-ethanol system at 25 °C, 50 % volume ethanol (b).

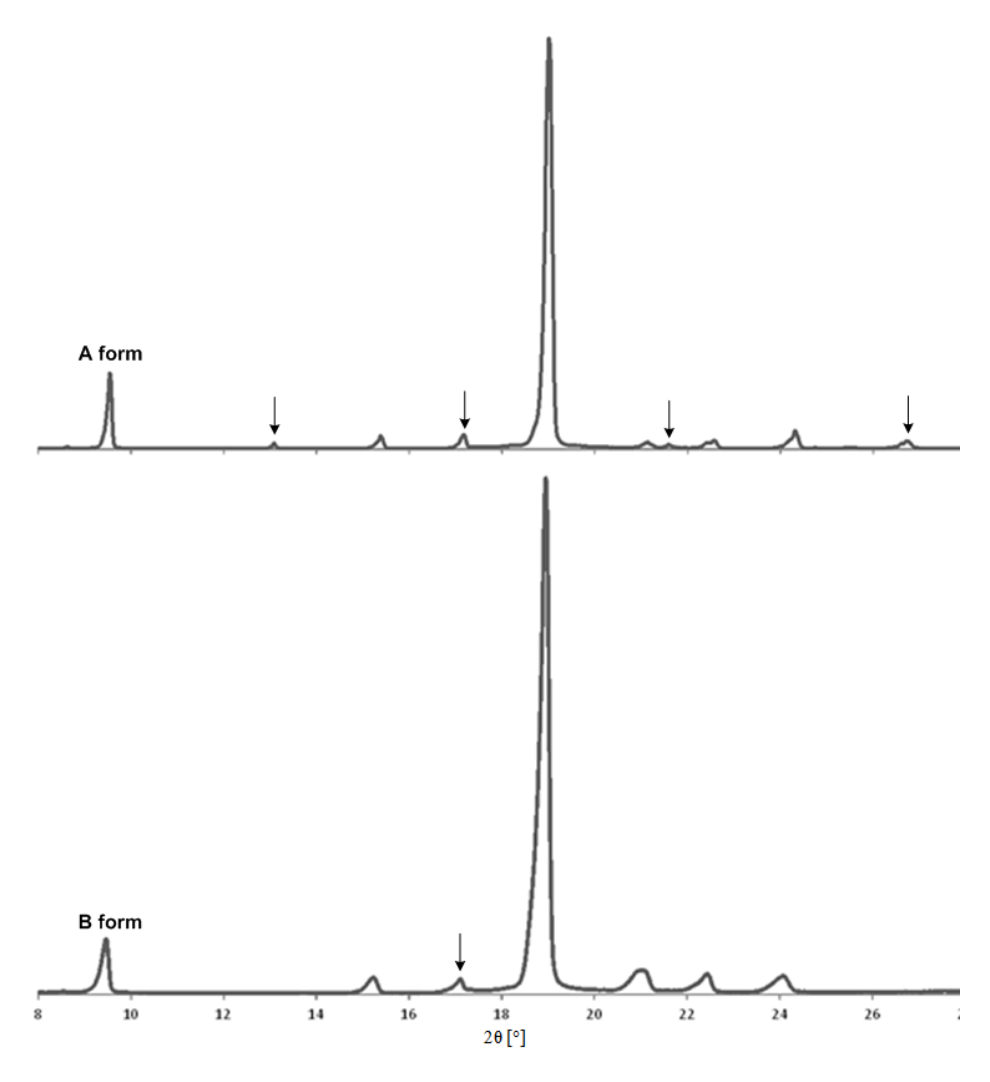


Figure 8. XRPD patterns of forms A and B.

4.3 Crystal Growth and Dissolution Rates Measurement

The growth rate of form A was determined via seeded batch desupersaturation experiments using time dependent measurements of both solute concentrations and particle size distributions (PSDs) (Garside et al., 2002; Wantha and Flood, 2011; Gougazeh et al., 2009). Experiments were performed at 10, 25, and 40 °C in a 0.5 L batch crystallizer (see Figure 9) agitated by a centrally located four-blade impeller driven by an overhead stirrer at 250 rpm. The solute concentration in the clear liquor sample was measured periodically using the refractive index method, and the crystal size distribution of crystalline samples was measured by analyzing a population of greater than 30 crystals under a microscope. Growth rate was determined as the time rate of change of the mean crystal size. To ensure that nucleation did not occur during the experiment the secondary nucleation thresholds were determined using a method described previously (Wantha and Flood, 2011), and the initial supersaturation for each growth experiment was performed within the metastable region. Nucleation was not detected by the naked eye in any seeded batch crystallization for growth determination. In addition, analysis using optical microscopy did not detect any crystals smaller than the initial seed population at any time, again suggesting that nucleation did not occur during the experiment.

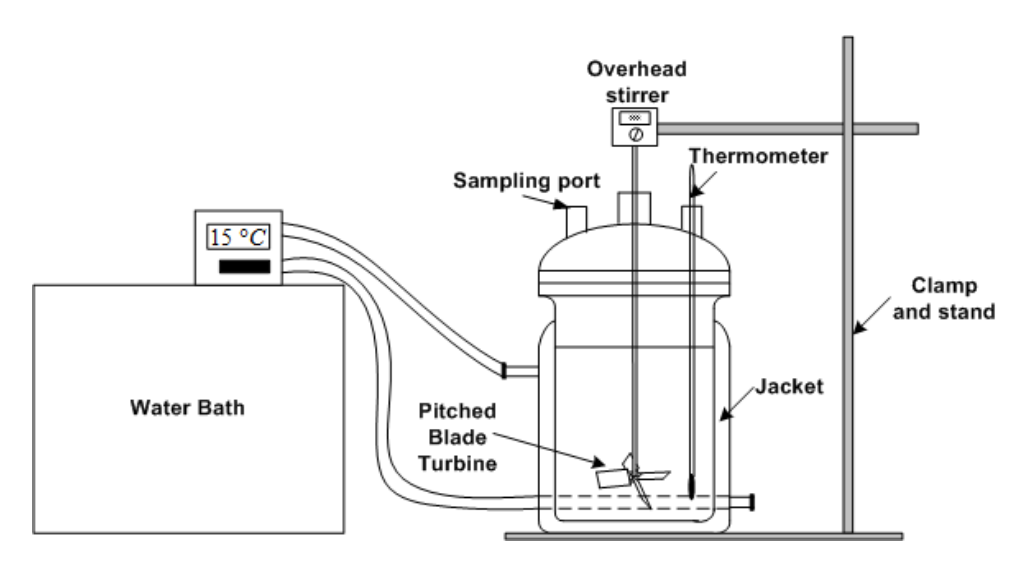


Figure 9. The 0.5 L Batch crystallizer.

Desupersaturation experiments were performed on solutions that had previously been heated to 20 °C above the experimental temperature (this is also at least 5 °C above the saturation temperature) for 30 to 40 min to ensure that the solution is homogeneous, and that there was no ghost nuclei remaining in the solution. The solutions were then cooled to the experimental temperature, and when the temperature reached the experimental temperature, a quantity of dry seed was fed to the crystallizer. A small volume of the suspension was sampled at specific times, and filtered quickly before determination of the crystal size distribution and solute concentration.

Deundersaturation experiments for determining the dissolution rates of form B were studied using a similar method to the growth experiments, except the experiments were performed at 10, 25, and 40 °C, and under the solubility of form B.

All dry crystal samples were obtained quickly by vacuum filtration (using a membrane with a pore size of $0.45~\mu m$) of a suspension sample and were washed with cold ethanol to remove water at the crystal surface. The crystal products were suspended in a saturated ethanol solution at ambient temperature, and a solution droplet was placed on a cover slip under a microscope. The population of crystals was recorded with a micrograph and the crystal size distributions were measured from the photomicrographs. The two largest visible lengths of each crystal were observed and the crystal size was calculated from the geometric mean of these two lengths. The micrographs were calibrated using a standard, and the number of crystals measured in each sample was greater than 30.

The solubility data of form A and form B in water were obtained from a previous study (Kitamura, 1993). To analyze the repeatability of experimental results, each kinetic measurement was performed at least three times.

4.4 Induction Time Measurement

Nucleation mechanisms were determined via the induction time measurement method. Induction time measurements of L-his in the water-ethanol solution were

performed at 25 °C in a 0.25 L batch crystallizer (see Figure 10). A series of saturated solution (aqueous solution of L-his) was prepared and heated to 5 °C above saturation temperature for 30 to 40 min to ensure that no ghost nuclei remained in the solution. Then the solution was cooled to experimental temperature and kept at this temperature. When the temperature reached the experimental temperature, ethanol was added to the solution. The induction time was then measured by recording the appearance of the crystals by eye. Three reproducible experiments were carried out for the different supersaturation levels tested. The crystals obtained at the initial stage of crystallization were characterized by microscope and XRPD.

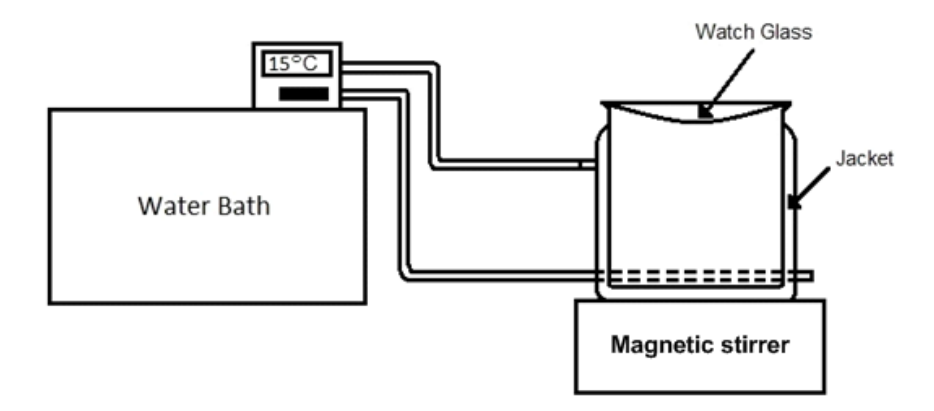


Figure 10. The 0.25 L Batch crystallizer.

5. Results and Discussion

Photomicrographs of seed crystals and product crystals from a growth experiment of form A of L-his at 25 °C are shown in Figure 11. This figure shows that there is no nucleation occurring during the growth process because no particles smaller than the seed crystals are detected. The obtained crystal size distribution (CSD) also confirmed this. The distribution was accurate because the photos were calibrated using a standard and a large sample (> 30 crystals) was used. The shape of all crystals from the growth experiments is a rod-like shape which confirms that the seed and product crystals are form A. After the growth process the concentration reaches the solubility of

form A and then remains constant, as shown in Figure 12. This indicates that there was no phase transformation during the growth processes of form A.

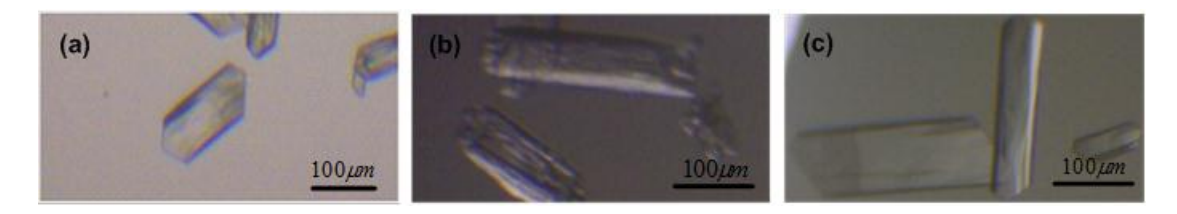


Figure 11. Photomicrographs of seed crystals and product crystals at various times from the growth experiment of form A at 25 °C: seed (a), 30 min (b), 100 min (c).

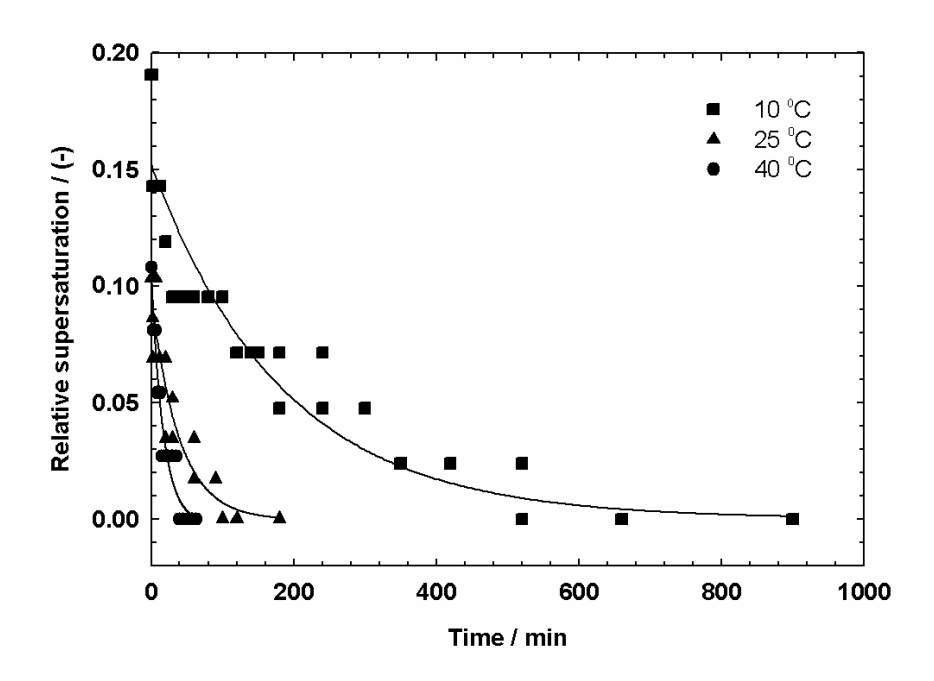


Figure 12. Desupersaturation curves from a batch run at different temperatures.

Photomicrographs of seed crystals and product crystals from a dissolution experiment of form B of L-his at 25 °C are shown in Figure 13. In this research the dissolution experiments were performed for relatively short batch times to avoid the transformation process. The shape of all crystals from the dissolution experiments is a plate-like, which confirms that the seed and product crystals are form B. After the dissolution process the concentration reaches the solubility of form B and then remains constant for some period of time, as shown in Figure 14. This also confirms that there

was no phase transformation during dissolution of form B during the relatively short batch times used (*ca* 30 min). If the crystals remained in solution for an extended period the concentration would drop to the solubility of form A due to the transformation of form B into form A.

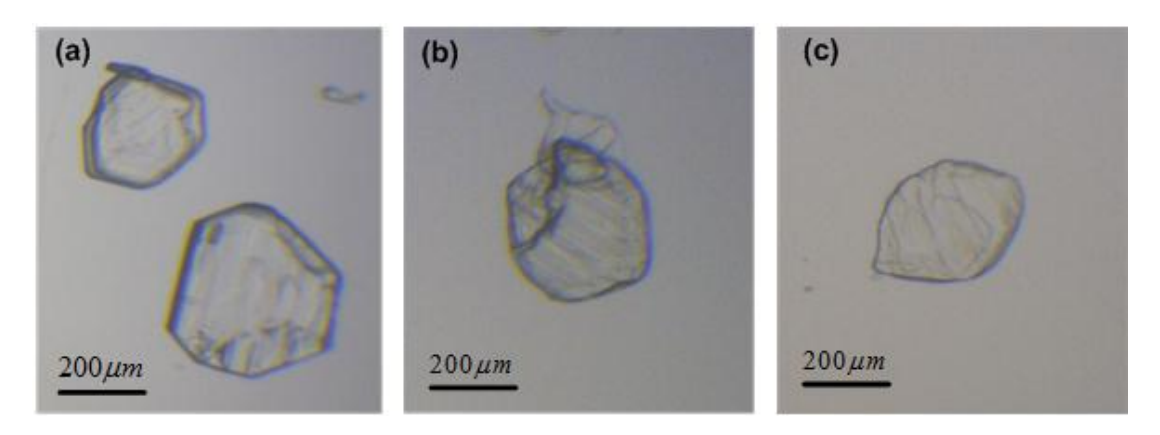


Figure 13. Photomicrographs of seed crystals and product crystals at various times from the dissolution experiment of form B at 25 °C: seed (a), 5 min (b), 13 min (c).

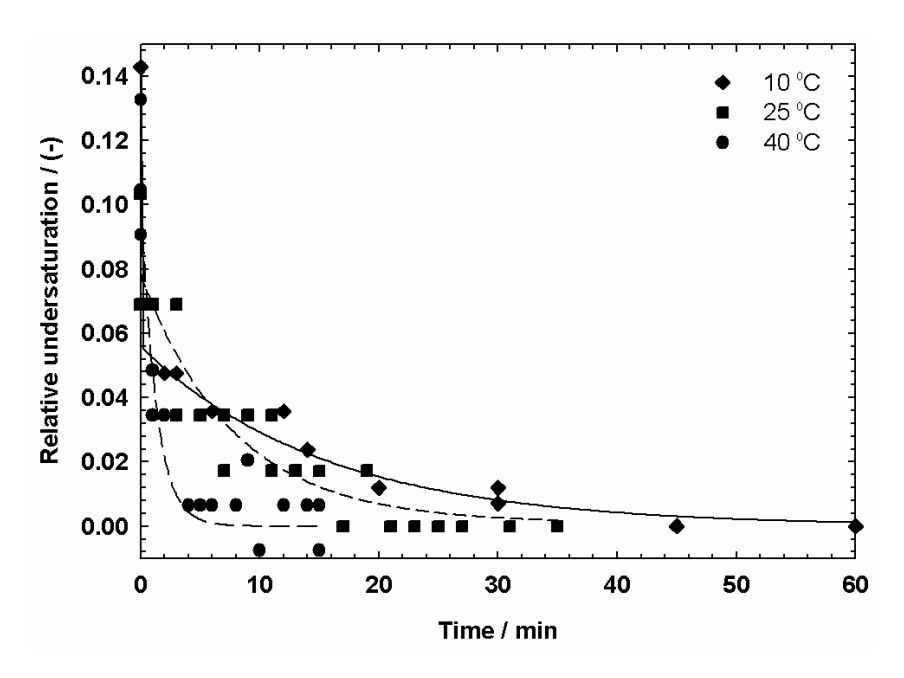


Figure 14. Deundersaturation curves from a batch run at different temperatures.

Figure 12 shows the desupersaturation curves from the growth experiments of form A. The desupersaturation rate increases with increasing temperature since both the

rate of mass transfer and the rate of integration of solute into the crystal surface increase with increasing temperature. This indicates that the growth rate of form A increases with increasing temperature as expected (see further in Figure 16). Figure 14 shows that the rate of the reduction of the undersaturation increases with increasing temperature, which indicates the dissolution rates of form B increases with increasing temperature as expected (see further in Figure 18).

The crystal size distributions (CSDs) were measured from micrographs of samples taken at particular times. The counted number of crystals for each sample was greater than 30. The number mean crystal size was determined by the total crystal length divided by total counted number of crystals. The number mean crystal size was used to calculate the growth rate because the growth rate data can only be obtained from batch growth using the population balance, which is a number-based balance. If the volume or mass mean sizes are used then the result is not suitable for use in the population balance, and therefore far less useful. The growth and dissolution rates can be calculated from the change of the mean crystal size divided by the change of the time of each measurement, with these being correlated with the average of the measured supersaturation at the same time. In this research the change of mean crystal sizes with time is fitted with any continuous function that fits the data well, and then the mean growth and dissolution rates were calculated by the following definition

$$\overline{G}(t) = \frac{d\overline{L}}{dt} \tag{10}$$

$$\overline{G}(t) = \frac{d\overline{L}}{dt} \bigg|_{t}$$

$$\overline{D}(t) = -\frac{d\overline{L}}{dt} \bigg|_{t}$$
(10)

where \overline{L} is mean crystal size (µm) and t is time (min). $\overline{G}(\sigma_G)$ and $\overline{D}(\sigma_D)$ can then be found from G(t) and D(t), respectively, using the measured concentration data as a function of time.

Figure 15 shows the desupersaturation curves and time dependence of mean crystal sizes of form A for the experiments at 25 °C. An exponential decay fits all of the supersaturation data very well. This equation is given by Eq. (12):

$$\sigma_G = 0.0960e^{-0.0258t} \tag{12}$$

Numerical constants in the fitted functions were not rounded to avoid error propagation when applying further calculations to the final crystal growth rate model. An exponential rise to a maximum fits all of the mean crystal size (in µm) data well, and the equation is given by Eq. (13):

$$\overline{L} = 203 + 92\left(1 - e^{-0.0308t}\right) \tag{13}$$

The mean growth rate is determined as the first derivative of mean crystal sizes (Eq. (13)) with respect to time, which is given by Eq. (14).

$$\overline{G} = \frac{d\overline{L}}{dt} = 2.832e^{-0.0308t} \tag{14}$$

The growth rates were calculated using the mean crystal size. The crystal growth experiments allowed growth rates (Eq. (14)) to be determined as a function of relative supersaturation (Eq. (12)), as shown in Figure 16. The growth rates at 10 and 40 °C are determined using the same method, and the results are shown in Figure 16. It can be seen that, at constant temperature, the growth rates increase with increasing supersaturation. This figure also indicates that the growth rate are strongly temperature dependent.

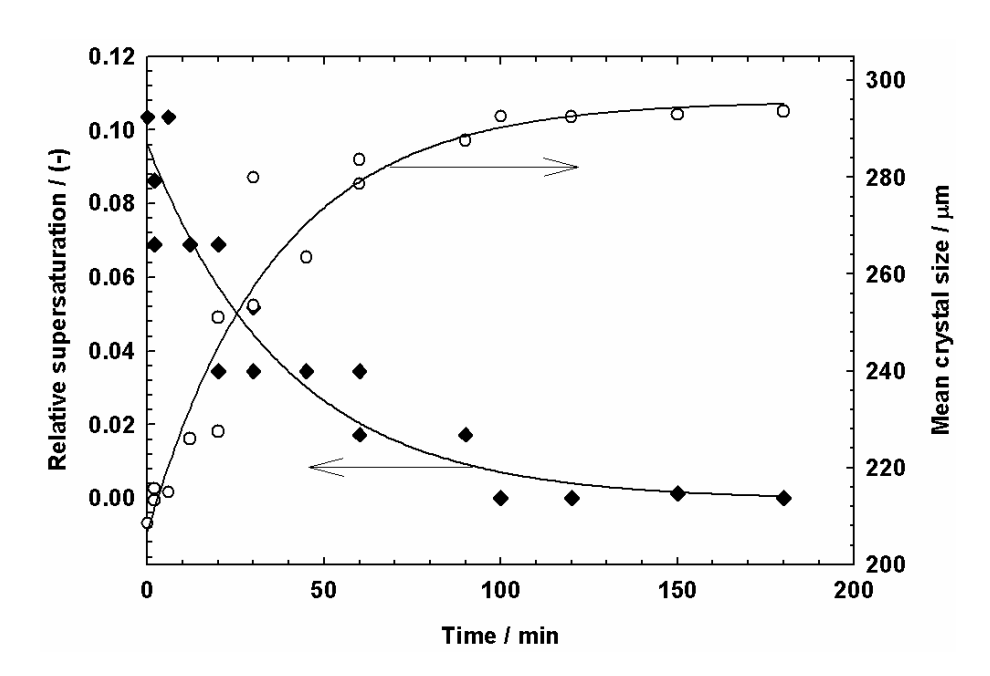


Figure 15. Desupersaturation curves and time dependence of crystal sizes of form A for the experiments at 25 °C.

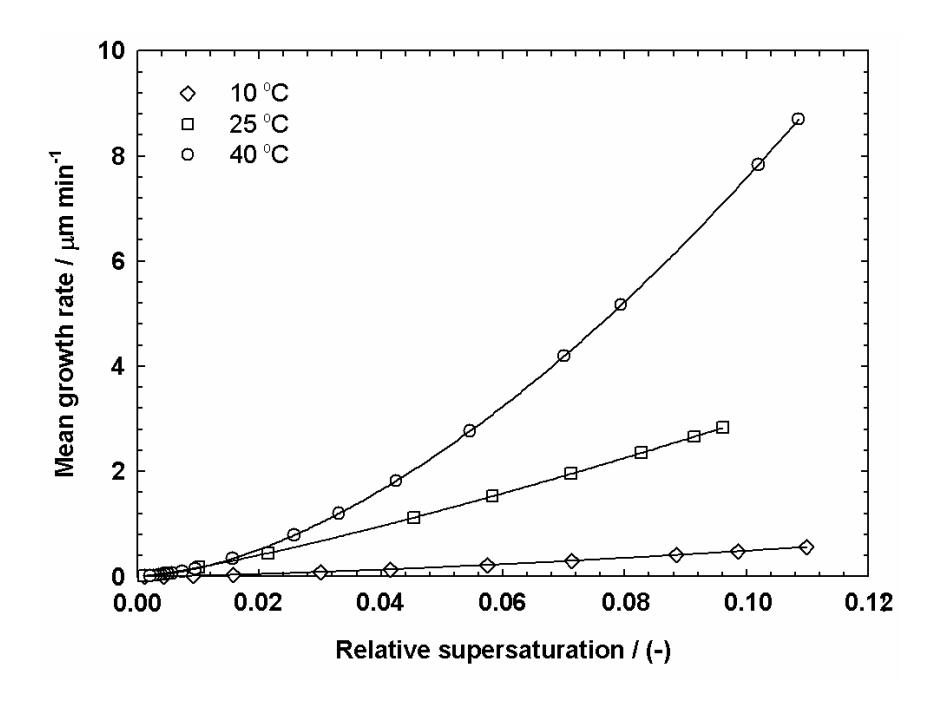


Figure 16. Mean growth rates for form A as a function of relative supersaturation.

Figure 17 shows deundersaturation curves and time dependence of crystal sizes of form B for the experiments at 25 °C. An exponential decay fits all of the deundersaturation data well. This equation is given by Eq. (15):

$$\sigma_D = 0.0706e^{-0.1050t} \tag{15}$$

An exponential decay also fits all of the mean crystal size data well, and the equation is given by Eq. (16):

$$\overline{L} = 246 + 185e^{-0.1035t} \tag{16}$$

The mean dissolution rate is determined as the first derivative of mean crystal sizes (Eq. (16)) with respect to time, which is given by Eq. (17).

$$\overline{D} = -\frac{d\overline{L}}{dt} = 19.11e^{-0.1035t}$$
 (17)

The dissolution rates were calculated using the mean crystal size. The dissolution experiments allowed dissolution rates (Eq. (17)) to be determined as a function of relative undersaturation (Eq. (15)), as shown in Figure 18. The dissolution rates at 10 and 40 °C are determined using the same method, and the results are shown in Figure 18. It can be seen that, at constant temperature, the crystal dissolution rates increase with increasing undersaturation. At constant undersaturation, the dissolution rates increase with increasing temperature.

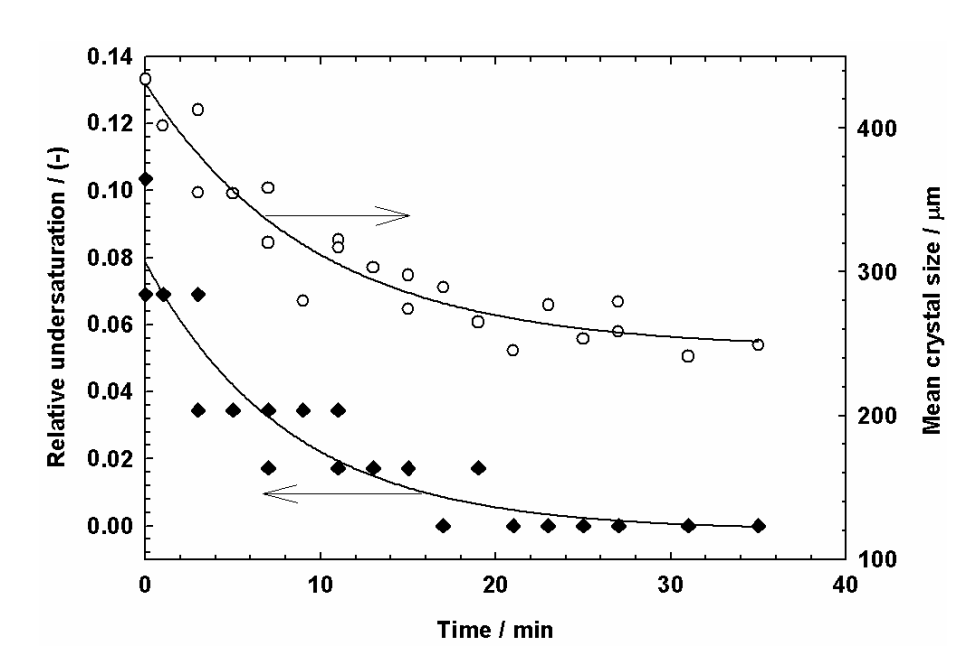


Figure 17. Deundersaturation curves and time dependence of crystal sizes of form B for the experiments at 25 °C.

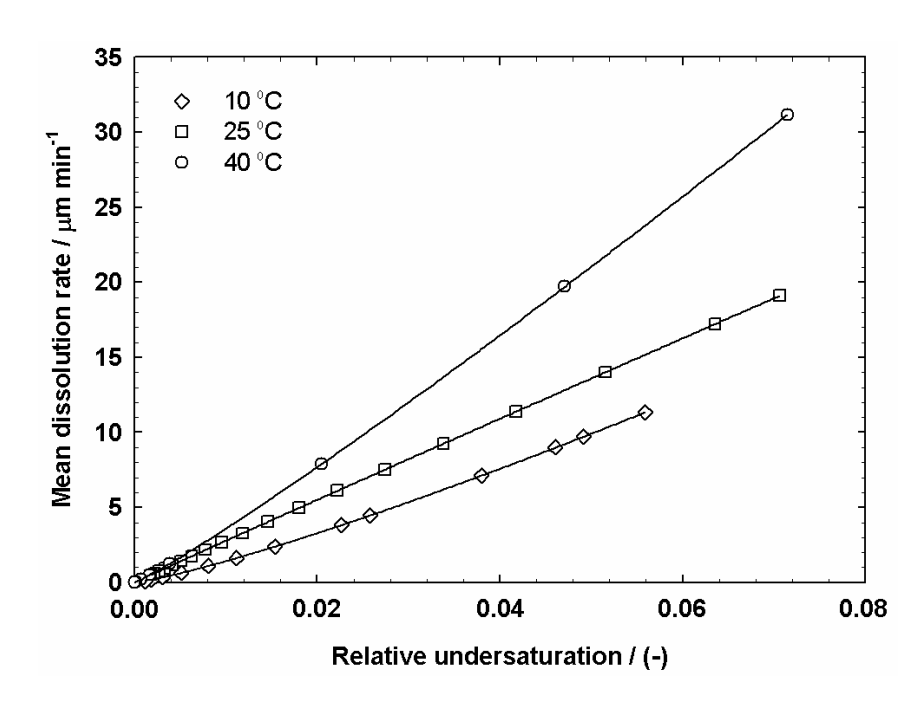


Figure 18. Mean dissolution rates for form B as a function of relative undersaturation.

The growth (or dissolution) kinetics can be expressed as a function of supersaturation (or undersaturation) for each set of conditions by the power-law model (Gougazeh et al., 2009)

$$\overline{G} = \frac{d\overline{L}}{dt} = k_G \sigma_G^g \tag{18}$$

$$\overline{D} = -\frac{d\overline{L}}{dt} = k_D \sigma_D^d \tag{19}$$

where \overline{G} and \overline{D} are the mean growth and dissolution rates (µm min⁻¹), respectively; k_G and $k_{\rm D}$ are the growth and dissolution rate constants ($\mu {\rm m~min}^{-1}$); ${\pmb \sigma}_{\rm G}$ and ${\pmb \sigma}_{\rm D}$ are the relative supersaturation and undersaturation; and n and m are the growth and dissolution rate orders, respectively. The experimental results of the growth of form A and dissolution of form B were fitted with Eqs. (18) and (19) using the fitting routine from the software Sigmaplot 13.0, and the results are shown in Figs. 19, 20, and 21. 95% confidence intervals for each parameter in the model are given by the fitting routine and are presented along with the values of the parameters in Table 1. The value of the growth rate order is used in understanding of the controlling mechanism. In general a growth rate order of g = 1 indicates that mass transfer becomes a rate controlling mechanism and a growth rate order between 1 and 2 indicate surface integration step is at least partially rate controlling (Mullin, 2001). It can be seen that in the case of the growth of form A the growth orders are 1.44 \pm 0.062, 1.23 \pm 0.14, and 1.67 \pm 0.02, respectively, for 10, 25, and 40 °C. This indicates that the surface integration process plays an important role in explaining the growth process of form A. For the case of the dissolution of form B, the dissolution rate orders are 1.21 \pm 0.10, 0.98 ± 0.05 , and 1.10 ± 0.23 , respectively, for 10, 25, and 40 °C. This indicates that at 25 and 40 °C the mass transfer process plays an important role in explaining the dissolution process of form B, and at 10 °C the surface disintegration is also important.

In crystallization of polymorphs from solution, the SMT is usually the most important process which describes the transformation from the metastable polymorph to the stable polymorph. A SMT from form B to form A will take place when crystals of form B are nucleated in, or put into a saturated aqueous solution. The dissolution of form B and growth of form A are the main kinetics of SMT. As shown in Fig. 19 the dissolution kinetics of form B are faster than the growth kinetics of form A. This leads to the SMT of form B into form A being a growth controlled process. This means that the mass transfer of solute from the crystal surface to the bulk solution (due to the dissolution of form B) rapidly proceeds to maintain the solute concentration at or close to the solubility of form B. However, the growth of form A and dissolution of form B occur simultaneously during SMT until form B crystals are completely dissolved, which means that the transformation is complete. Then the concentration will drop slowly to the solubility of form A due to the growth of form A. This conclusion agrees with the previous SMT study of L-his by Kitamura (1993). In the literature there are a lot of studies showing that the growth of the stable polymorph is the limiting step, for example L-glutamic acid (Dharmayat et al., 2008; Garti et al., 1997; Ono et al., 2004), taltireline (Maruyama et al., 1999), and carbamazepine (O'Mahony et al., 2012; Qu et al., 2006). The SMT of DL-methionine (Wantha and Flood, 2013a) and glycine (Ferrari et al., 2003) are at least two examples where the dissolution of the metastable polymorph was the limiting step.

Table 1. Results from kinetics parameter estimation at a 95% confidence level.

T (°C)	Growth of from A		Dissolution of form B	
	k_G (µm min ⁻¹)	g [-]	$k_D (\mu \mathrm{m min}^{-1})$	d [-]
10	13.64 ± 3.123	1.44 ± 0.062	366.4 ± 62.44	1.21 ± 0.10
25	50.69 ± 8.143	1.23 ± 0.14	260.0 ± 7.589	0.98 ± 0.05
40	352.8 ± 24.09	1.67 ± 0.02	566.6 ± 139.6	1.10 ± 0.23

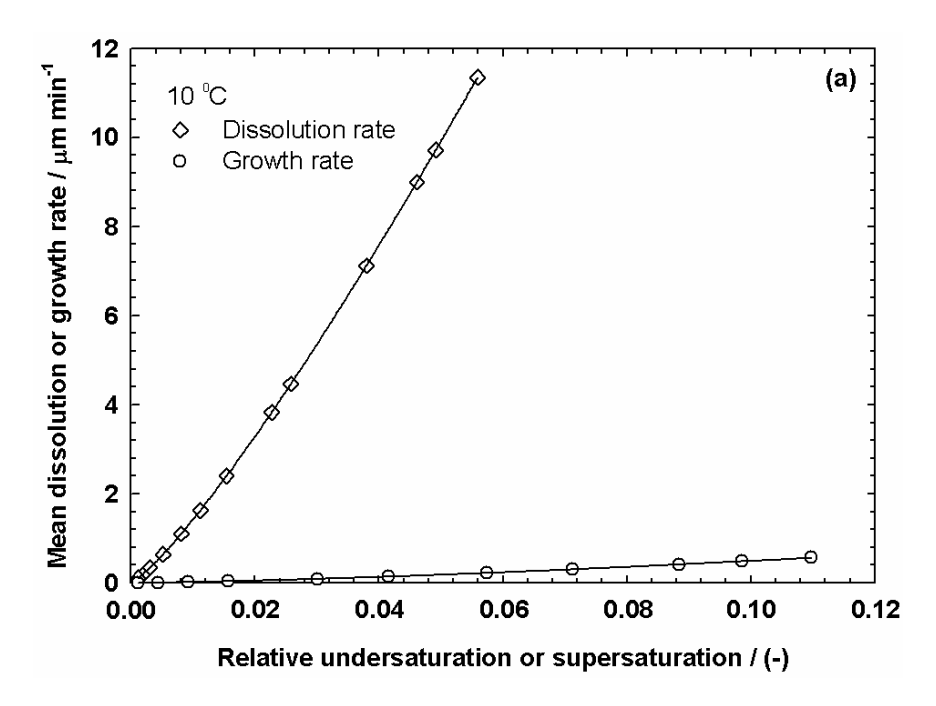


Figure 19. Mean growth rates for form A and dissolution rates for form B as a function of relative supersaturation and undersaturation at 10 °C.

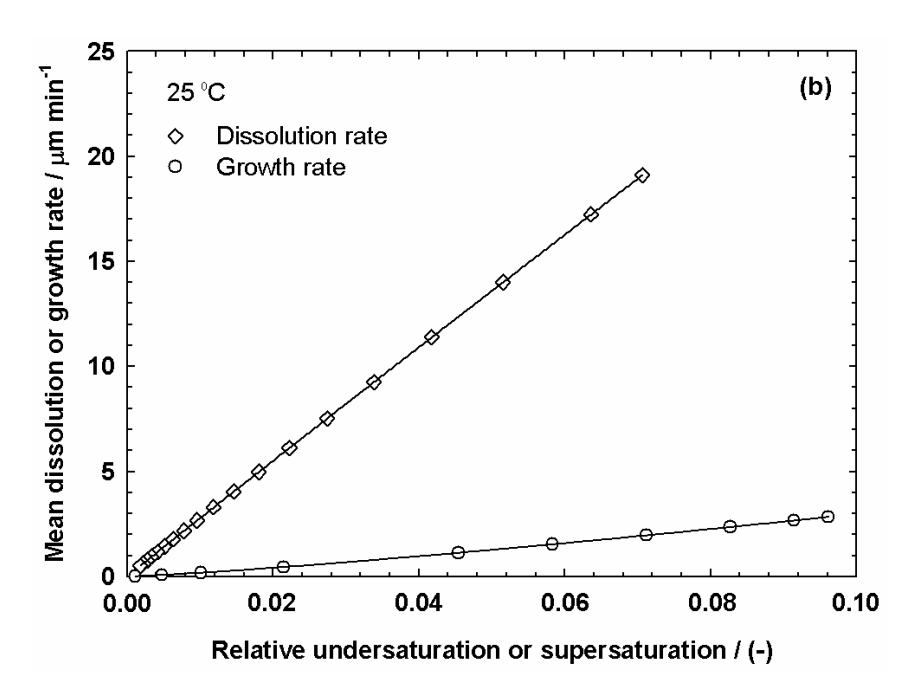


Figure 20. Mean growth rates for form A and dissolution rates for form B as a function of relative supersaturation and undersaturation at 25 °C.

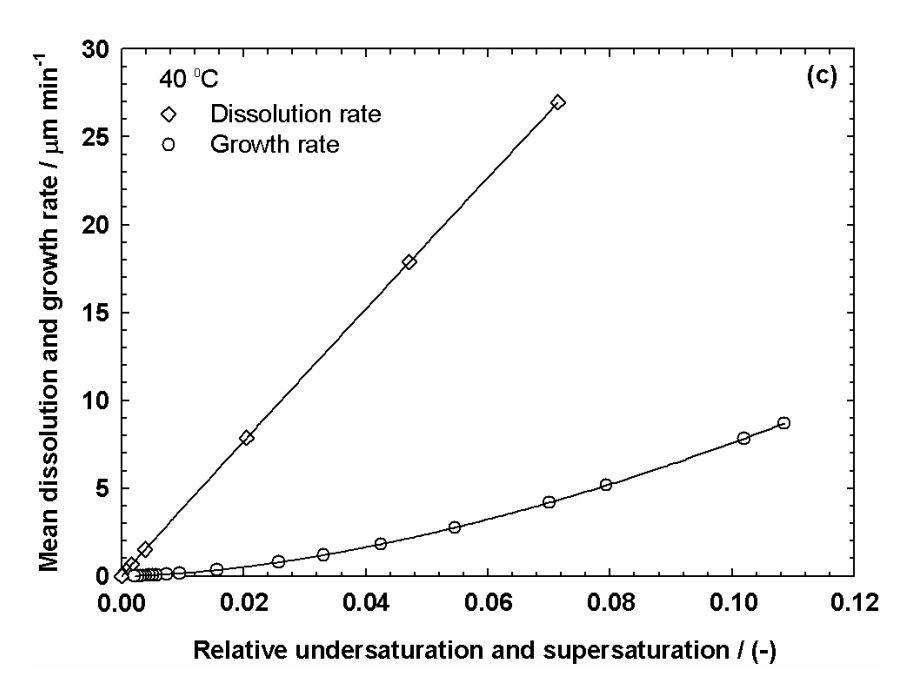


Figure 21. Mean growth rates for form A and dissolution rates for form B as a function of relative supersaturation and undersaturation at 40 °C.

The induction times of B polymorph of L-his in the water-ethanol solution are shown Figure 22. Each point represents the mean of experimental data at least three measurements. It can be observed that the induction time decreases with increasing supersaturation ratio. The numbers in the bracket represent the volume fraction of ethanol added to the solution. It can be observed that the induction time decreases with the increasing fraction of ethanol. This indicates that the nucleation rate of L-his increases with an increasing supersaturation ratio and fraction of ethanol. The nucleation kinetic of the metastable form B is one of the important parameters for characterization of the polymorphic transformation of L-his.

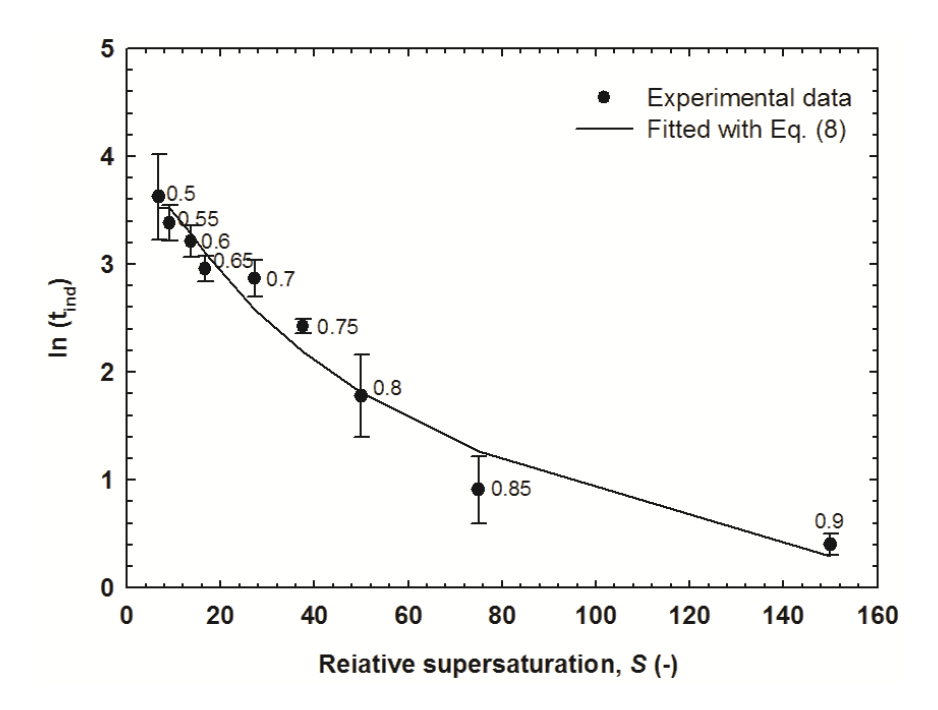


Figure 22. Measured induction times as a function of supersaturation ratio for different volume fraction of ethanol added at 25 °C. Numbers in the bracket represent the volume fraction of ethanol added.

A plots of $\ln(t_{ind})$ against $1/(\ln S)^2$ of the nucleation experiments of B polymorph of L-his in aqueous-ethanol solution at 25 °C are shown in Figure 23. The result shows that the fitted line with Eq. (2) is not very good ($R^2 = 0.6747$). However, Mullin (2001) suggested that the line would be separated into two straight lines corresponding to the mechanisms of homogeneous and heterogeneous nucleation. This plot is shown in Figure 24. This result is similar to other research that has been reported previously (Schöll et al., 2006; Zhi et al., 2011). The results show that the measured nucleation kinetics follow the trends expected from the CNT. The best-fit values of A_m and B are shown in Table 2.

These two lines are separated based on the system nucleating at low and high supersaturations. The shorter induction time was recorded as supersaturation increases. This is probably because a higher solution supersaturation effectively reduces the size of critical nucleus, and hence, shortens the induction time. Moreover, the results show that at a higher solution concentration, the onset of crystallization

occurs at a shorter induction period. A higher supply of fresh solution at higher solution concentrations results in a prolonged lifetime of nuclei, which then enhances the crystal growth.

The measured nucleation kinetics follows the trends expected from CNT. As indicated in Table 2 (mononuclear mechanism), the lowest coefficient of determinations, R^2 , is 0.96. This means that the correlation between the induction time and Eq. (2) is not very good.

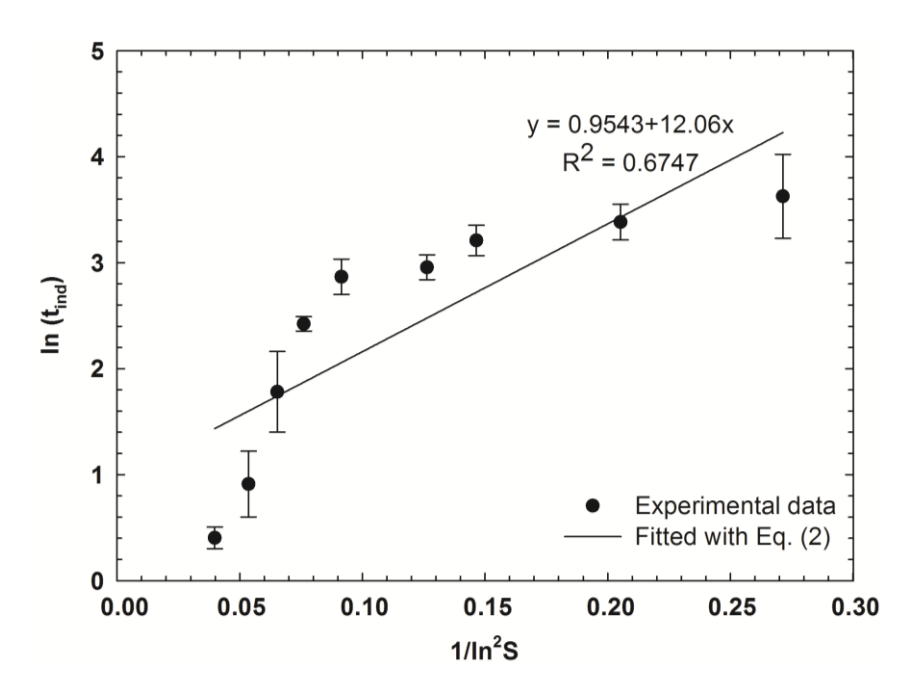


Figure 23. Dependence of induction time on supersaturation ratio of B polymorph of L-his in water-ethanol solution at 25 °C. Data are fitted using Eq. (2).

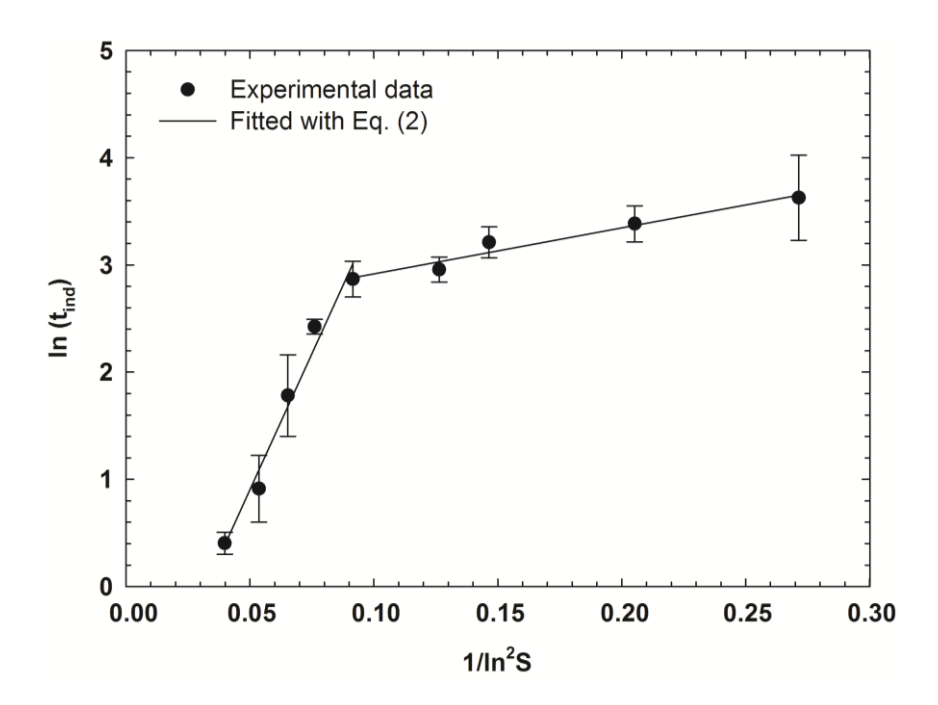


Figure 24. Dependence of induction time on supersaturation ratio of B polymorph of L-his in water-ethanol solution at 25 °C. Data are fitted using Eq. (2). The fitted line is separated into two straight lines.

Table 2. Parameters and coefficient of determination in Eq. (2).

Nucleation	Eq. (2)		
	A_m	В	R^2
Homogeneous	-1.636	50.75	0.9763
Heterogeneous	2.488	4.285	0.9603

In comparison with the polynuclear mechanism, it is necessary to correlate the induction time with Eq. (8). Parameters and the coefficient of determinations in Eq. (8) are listed in Table 3. A plots of $\ln(t_{ind})$ against $1/(\ln S)^2$, and data are fitted using Eq. (8) as shown in Figure 25.

It can be seen from Table 3 that the coefficient of determination, R^2 , is above 0.99. This means that the correlation between the induction time and Eq. (8) is very good. This indicates that nucleation mechanism of B polymorph of L-his in the water-

ethanol system at 25 °C is governed by the polynuclear mechanism, where the metastability is lost by nucleation and growth of nuclei. Moreover, g = 1.81 indicates that the growth of B polymorph of L-his in the water-ethanol system at 25 °C is a "birth and spread" growth mechanism, which belongs to the two-dimensional nucleation-mediated growth (Myerson, 2001).

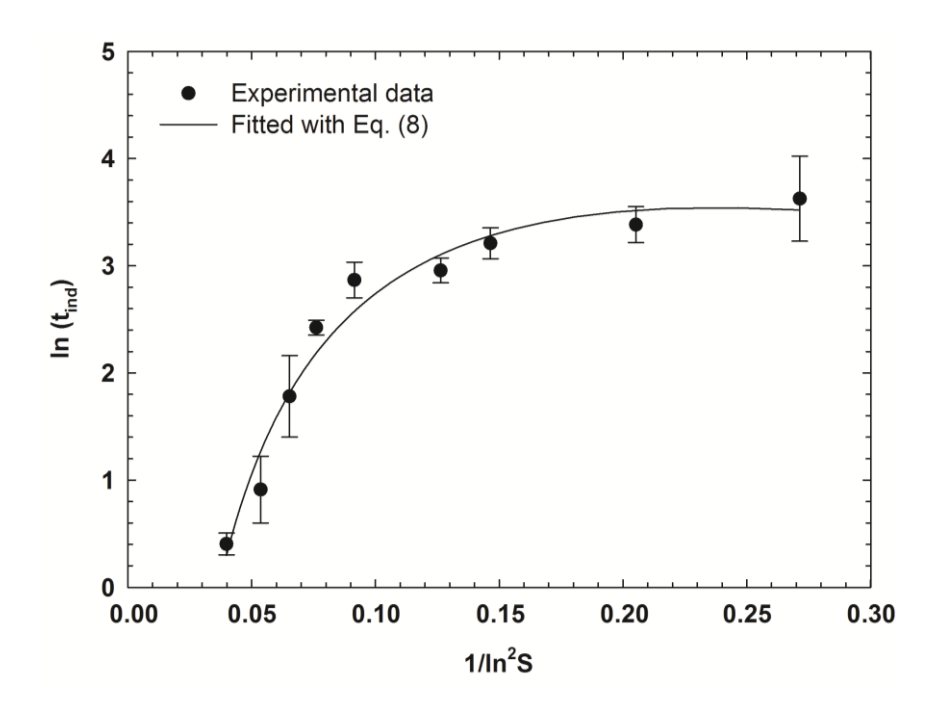


Figure 25. Dependence of induction time on supersaturation ratio of B polymorph of L-his in water-ethanol solution at 25 °C. Data are fitted using Eq. (8).

Table 3. Parameters and coefficient of determination in Eq. (8).

Parameters	$\ln A_P$	В	g	R^2
	8.299	-22.28	1.810	0.9926

Figure 26 shows a typical change in the XRPD patterns of the initial product crystals relative to the fraction of ethanol for crystallization at 25 °C. It can be seen that the characteristic peaks of each polymorph change with fraction of ethanol because of the generation of polymorphs B or a mixture of polymorphs A and B. From Figure 26, the characteristic peaks at ethanol volume fraction of 0.5, 0.7, and 0.9 are the peaks for

polymorph B. This indicates that the crystals obtained at the initial stage of crystallization were polymorph B. At ethanol volume fraction of 0.3 and 0.4 the characteristic are the peaks for a mixture of polymorphs A and B. This indicates that the crystals obtained at the initial stage of crystallization were a mixture of polymorphs A and B. All the results are shown Table 4. This table shows that the crystallization at temperature of 25 °C the polymorph B was obtained when ethanol volume fraction was greater than 0.5 ($S_A \ge 6.818$).

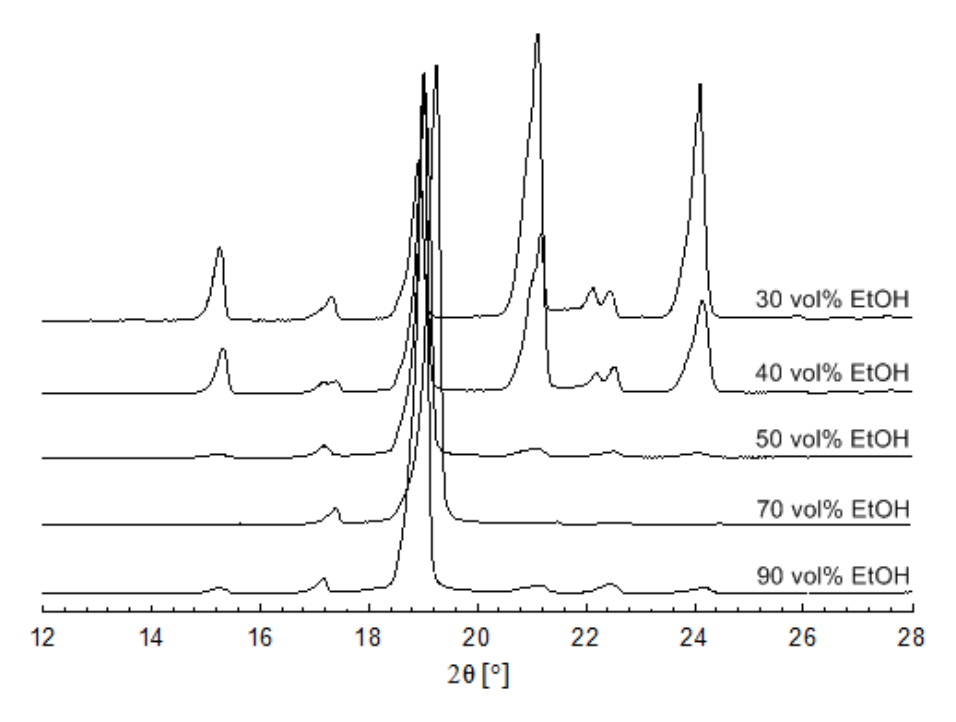


Figure 26. XRPD patterns of the crystals obtained at various ethanol volume fractions for temperature of 25 °C.

Table 4. Effect of ethanol on crystallization behavior of L-his.

Temperature	Ethanol volume	Supersaturation,	Initial crystal
(°C)	fraction [-]	S _A [-]	form
25	0.30	2.368	A+B
	0.40	3.368	A+B
	0.50	6.818	В
	0.55	9.909	В
	0.60	13.63	В
	0.65	16.67	В
	0.70	27.27	В
	0.75	37.50	В
	0.80	50.00	В
	0.85	75.00	В
	0.90	150.0	В

6. Conclusions

The growth kinetics of form A and dissolution kinetics of form B were measured at 10, 25, and 40 °C in an agitated batch crystallizer. The results showed that both the growth and dissolution rates increase with increasing temperature. The growth of form A is a surface integration controlled process and dissolution of form B is a mass transfer controlled process except at low temperature. At all temperatures studied, the dissolution rate of form B is faster than the growth rate of form A. This indicates that the transformation is a growth controlled process.

The nucleation and growth mechanisms of form B were determined by the induction time measurements. The experimental data can be separated into two straight lines corresponding to the mechanisms of homogeneous and heterogeneous nucleation. Induction time increases with decreasing supersaturation and ethanol fraction. The

nucleation is governed by a polynuclear mechanism. The growth mechanism is twodimensional nucleation-mediated growth. A further nucleation mechanism for the form A will also be determined. This should allow a complete model of the SMT to be achieved.

For the effect of ethanol, the results showed that the crystals obtained at the initial stage of crystallization were polymorph B at higher ethanol volume fraction and supersaturation, and a mixture of polymorphs A and B at lower ethanol volume fraction and supersaturation.

Acknowledgements

The author acknowledges the financial support of the faculty of Engineering of Burapha University, Commission on Higher Education, and Thailand Research Fund, Thailand. XRPD support by the Frontier Research Center, Vidyasirimedhi Institute of Science and Technology, Thailand, is also gratefully acknowledged.

References

- [1] W. Beckmann, "Seeding the Desired Polymorph: Background, Possibilities, Limitations, and Case Studies", Org. Process Res. Dev. 4(5): 372-383 (2000).
- [2] W. Beckmann, and W.H. Otto, "Occurrence, Stability, Kinetics of Crystallization and Polymorphic Transition of the A, B and C Modification of Abecarnil - Influence of Supersaturation, Temperature, Solvents and Impurities", Chem. Eng. Res. Des. 74, 750-757 (1996).
- [3] J. Bernstein, R.J. Davey, and J.O. Henck, "Concomitant Polymorphs", Angew. Chem. Int. Ed. 38(23): 3440-3461 (1999).
- [4] R. Bobrovs, L. Seton, and A. Actinš, "Solvent-Mediated Phase Transformation Between Two Tegafur Polymorphs in Several Solvents", CrystEngComm. 16, 10581-10591 (2014).

- [5] S.J. Bonafede, and M.D. Ward, "Selective Nucleation and Growth of an Organic Polymorph by Ledge-Directed Epitaxy on a Molecular Crystal Substrate", J. Am. Chem. Soc. 117(30), 7853-7861 (1995).
- [6] J.S. Capes, and R.E. Cameron, "Contact Line Crystallization to Obtain Metastable Polymorphs", Cryst. Growth Des. 7(1), 108-112 (2006).
- [7] C. Cashell, D. Corcoran, and B.K. Hodnett, "Control of Polymorphism and Crystal Size of L-Glutamic Acid in the Absence of Additives", J. Cryst. Growth 273(1-2), 258-265 (2004).
- [8] J. Chen, B. Shama, J.M.B. Evans, and A.S. Myerson, "Pharmaceutical Crystallization", Cryst. Growth Des. 11(4), 887-895 (2011).
- [9] R.J. Davey, N. Blagden, G.D. Potts, and R. Docherty, "Polymorphism in Molecular Crystals: Stabilization of a Metastable Form by Conformational Mimicry", J. Am. Chem. Soc.119(7), 1767-1772 (1997).
- [10] S. Dharmayat, R.B. Hammond, X. Lai, C. Ma, E. Purba, K.J. Roberts, Z-P. Chen, E. Martin, J. Morris, and R. Bytheway, "An Examination of the Kinetics of the Solution-Mediated Polymorphic Phase Transformation between α- and β-Forms of I-Glutamic Acid as Determined Using Online Powder X-ray Diffraction", Cryst. Growth Des. 8(7), 2205-2216 (2008).
- [11] E.S. Ferrari, R.J. Davey, W.I. Cross, A.L. Gillon, and C.S. Towler, "Crystallization in Polymorphic Systems: The Solution-Mediated Transformation of β to α Glycine", Cryst. Growth Des. 3(1), 53-60 (2003).
- [12] G. Févotte, C. Alexandre, and S.O. Nida, "A Population Balance Model of the Solution-Mediated Phase Transition of Citric Acid", AIChE J. 53(10), 2578-2589 (2007).
- [13] J. Garside, A. Mersmann, and J. Nyvlt, Measurement of Crystal Growth and Nucleation Rates, 2nd ed., Institute of Chemical Engineering, London 2002.

- [14] N. Garti, and H. Zour, "The Effect of Surfactants On the Crystallization and Polymorphic Transformation of Glutamic Acid", J. Cryst. Growth 172(3-4), 486-498 (1997).
- [15] M. Gougazeh, W. Omar, and J. Ulrich, "Growth and Dissolution Kinetics of Potassium Sulfate in Pure Solutions and In the Presence of Cr³⁺ Ions", Cryst. Res. Technol. 44(11), 1205-1210 (2009).
- [16] D.J.W. Grant, "Theory and Origin of Polymorphism", In: H.G. Brittain (ed.).
 Polymorphism In Pharmaceutical Solids, Drugs and the Pharmaceutical Sciences
 Vol. 95 (pp 1-34). New York: Marcel Dekker (1999).
- [17] U.J. Griesser, A. Burger, and K. Mereiter, "The Polymorphic Drug Substances of the European Pharmacopoeia. Part 9. Physicochemical Properties and Crystal Structure of Acetazolamide Crystal Forms", J. Pharm. Sci. 86(3), 352-358 (1997).
- [18] C.-H. Gu, K. Chatterjee, V. Young Jr, and D.J.W. Grant, "Stabilization of Metastable Polymorph of Sulfamerazine by Structurally Related Additives", J. Cryst. Growth 235(1-4), 471-481 (2002).
- [19] A. Gutjahr, H. Dabringhaus, and R. Lacmann, "Studies of the Growth and Dissolution Kinetics of the CaCO₃ Polymorphs Calcite and Aragonite I. Growth and Dissolution Rates in Water", J. Cryst. Growth 158(3), 296-309 (1996).
- [20] S. Jiang, P.J. Jansens, and J.H. ter Horst, "Control Over Polymorph Formation of o-Aminobenzoic Acid", Cryst. Growth Des. 10(6), 2541-2547 (2010).
- [21] N.C.S. Kee, R.B.H. Tan, and R.D. Braatz, "Selective Crystallization of the Metastable α-form of L-Glutamic Acid Using Concentration Feedback Control", Cryst. Growth Des. 9(7), 3044-3051 (2009).
- [22] Y. Kim, S. Haam, Y.G. Shul, W-S. Kim, J.K. Jung, H-C. Eun, and K-K. Koo, "Pseudopolymorphic Crystallization of L-Ornithine-L-Aspartate by Drowning Out". Ind. End. Chem. Res. 42(4), 883-889 (2003).
- [23] M. Kitamura, "Crystallization Behavior and Transformation Kinetics of L-Histidine Polymorphs", J. Chem. Eng. Jpn. 26(3), 303-307 (1993).

- [24] M. Kitamura, "Controlling Factor of Polymorphism in Crystallization Process", J. Cryst. Growth. 237-239, 2205-2214 (2002).
- [25] M. Kitamura, H. Furukawa, and M. Asaeda, "Solvent Effect of Ethanol on Crystallization and Growth Process of L-Histidine Polymorphs", J. Cryst. Growth 141(1-2), 193-199 (1994).
- [26] M. Kitamura, and T. Ishizu, "Growth Kinetics and Morphological Change of Polymorphs of L-Glutamic Acid", J. Cryst. Growth 209(1), 138-145 (2000).
- [27] M. Kitamura, H. Konno, A. Yasui, and H. Masuoka, "Controlling Factors and Mechanism of Reactive Crystallization of Calcium Carbonate polymorphs from Calcium Hydroxide Suspensions", J. Cryst. Growth 236(1-3), 323-332 (2002).
- [28] M. Kitamura, and K. Nakamura, "Effects of Solvent Composition and Temperature on Polymorphism and Crystallization Behavior of Thiazole Derivative", J. Cryst. Growth 236(4), 676-686 (2002).
- [29] H.J.M. Kramer, and G.M. van Rosmalen, Crystallization. In: I.D., Wilson and C.F., Poole (ed.). Handbook of Methods and Instrumentation in Separation Science volume 2 (pp 1-20). London: Academic Press (2009).
- [30] A. Kuldipkumar, G.S. Kwon, and G.G. Zhang, "Determining the Growth Mechanism of Tolazamide by Induction Time Measurement", Cryst. Growth Des. 7, 234-242 (2007).
- [31] C. Lindenberg, and M. Mazzotti, "Effect of Temperature On the Nucleation Kinetics of α L-Glutamic Acid", J. Cryst. Growth 311(4), 1178-1184 (2009).
- [32] C. Lindenberg, M. Mazzotti, "Continuous Precipitation of L-Asparagine Monohydrate in a Micromixer: Estimation of Nucleation and Growth Kinetics", AIChE J. 57(4), 942-950 (2011).
- [33] J. Lu, Z. Li, and X. Jiang, "Polymorphism of Pharmaceutical Molecules: Perspectives on Nucleation", Front. Chem. Eng. China 4(1), 37–44 (2010).
- [34] J. Lu, X.-J. Wang, X. Yang, and C-B. Ching, "Polymorphism and crystallization of famotidine" Cryst. Growth Des. 7(9): 1590-1598 (2007).

- [35] D. Mangin, F. Puel, and S. Veesler, "Polymorphism in Processes of Crystallization in Solution: A Practical Review", Org. Process Res. Dev. 13(6), 1241-1253 (2009).
- [36] S. Maruyama, H. Ooshima, and J. Kato, "Crystal structures and solvent-mediated transformation of Taltireline polymorphs", Chem. Eng. J. 75(3), 193-200 (1999).
- [37] A. Mersmann, Crystallization technology handbook, 2nd ed., Marcel Dekker Inc., New York 2001.
- [38] N.A. Mitchell, and P.J. Frawley, "Nucleation Kinetics of Paracetamol–Ethanol Solutions from Metastable Zone", J. Cryst. Growth 312(19), 2740-2746 (2010).
- [39] C.A. Mitchell, L. Yu, and M.D. Ward, "Selective Nucleation and Discovery of Organic Polymorphs through Epitaxy with Single Crystal Substrates", J. Am. Chem. Soc. 123 (44), 10830-10839 (2001).
- [40] R. Mohan, K.-K. Koo, C. Strege, and A.S. Myerson, "Effect of additives on the transformation behavior of L-phenylalanine in aqueous solution", Ind. Eng. Chem. Res. 40(26), 6111-6117 (2001).
- [41] J.W. Mullin, Crystallization, 4th ed., Butterworth-Heinemann, Oxford 2001.
- [42] A.S. Myerson, Handbook of industrial crystallization, 2nd ed., Elsevier Science & Technology Books, Amsterdam 2001.
- [43] Z.K. Nagy, M. Fujiwara, X.Y. Woo, and R.D. Braatz, "Determination of the Kinetic Parameters for the Crystallization of Paracetamol from Water Using Metastable Zone Width Experiments", Ind. Eng. Chem. Res. 47(4), 1245-1252 (2008).
- [44] M.A. O'Mahony, M. Anthony, D.M. Croker, Å.C. Rasmuson, and B.K. Hodnett, "Examining Solution and Solid State Composition for the Solution-Mediated Polymorphic Transformation of Carbamazepine and Piracetam", Cryst. Growth Des. 12(4), 1925-1932 (2012).
- [45] T. Ono, H.J.M. Kramer, J.H. ter Horst, and P.J. Jansens, "Process Modeling of the Polymorphic Transformation of I-Glutamic Acid", Cryst. Growth Des. 4(6), 1161-1167 (2004).

- [46] P. Pantaraks, and A.E. Flood, "Effect of Growth Rate History on Current Crystal Growth: A Second Look at Surface Effects on Crystal Growth Rates", Cryst. Growth Des. 5(1), 365-371 (2005).
- [47] M.M. Parmar, O. Khan, L. Seton, and J.L. Ford, "Polymorph Selection with Morphology Control Using Solvent", Cryst. Growth Des. 7(9), 1635-1642 (2007).
- [48] M. Prashad, P. Sutton, R. Wu, B. Hu, J. Vivelo, J. Carosi, P. Kapa, and J. Liang, "Process Research and Development of a MTP Inhibitor: Another Case of Disappearing Polymorphs upon Scale-up", Org. Proc. Res. Dev. 14(4), 878–882 (2010).
- [49] H. Qu, M. Louhi-Kultanen, J. Rantanen, and J. Kallas, "Solvent-Mediated Phase Transformation Kinetics of an Anhydrate/Hydrate System", Cryst. Growth Des. 6(9), 2053-2060 (2006).
- [50] A.D. Randolph, and M.A. Larson, Theory of Particulate Processes: Analysis and Techniques of continuous Crystallization, 2nd ed., Academic Press, California 1988.
- [51] C.P.M. Roelands, S. Jiang, M. Kitamura, J.H. ter Horst, H.J.M. Kramer, and P.J. Jansens, "Antisolvent Crystallization of the Polymorphs of I-Histidine as a Function of Supersaturation Ratio and of Solvent Composition", Cryst. Growth Des. 6(4), 955-963 (2006).
- [52] J. Schöll, C. Lindenberg, L. Vicum, J. Brozio, and M. Mazzotti, "Precipitation of α L-glutamic acid: determination of growth kinetics", Faraday Disccuss. 136, 247-264 (2007).
- [53] J. Schöll, L. Vicum, M. Muller, and M. Mazzotti, "Precipitation of L-Glutamic Acid: Determination of Nucleation Kinetics", Chem. Eng. Technol. 29, 257-264 (2006).
- [54] S. Srisa-nga, A.E. Flood, and E.T. White, "The Secondary Nucleation Threshold and Crystal Growth of α-Glucose Monohydrate in Aqueous Solution", Cryst. Growth Des. 6(3), 795-801 (2006).

- [55] G.W. Stowell, R.J. Behme, S.M. Denton, I. Pfeiffer, F.D. Sancilio, L.B. Whittall, and R.R. Whittle, "Thermally-Prepared Polymorphic Forms of Cilostazol", J. Pharm. Sci. 91(12), 2481-2488 (2002).
- [56] S. Suarez, L. Garcia-Contreras, and D. Sarrubi, "Facilitation of Pulmonary Insulin Absorption by H-Map: Pharmacokinetics and Pharmacodynamics in Rats", Pharm. Res. 18: 1677-1683 (2001).
- [57] S. Teychené, and B. Biscans, "Nucleation Kinetics of Polymorphs: Induction Period and Interfacial Energy Measurements", Cryst. Growth Des. 8(4), 1133-1139 (2008).
- [58] J. Ulrich, and P. Frohberg, "Problems, Potentials and Future of Industrial Crystallization", 19th International Workshop on Industrial Crystallization, (2012).
- [59] F. Wang, J.A. Wachter, F.J. Antosz, and K.A. Berglund, "An Investigation of Solvent-Mediated Polymorphic Transformation of Progesterone Using in Situ Raman Spectroscopy", Org. Process Res. Dev. 4(5), 391-395 (2000).
- [60] L. Wantha, Polymorphism and Solution-Mediated Transformation of DL-Methionine.
 Ph.D. Thesis, Suranaree University of Technology 2011.
- [61] L. Wantha, and A.E. Flood, "Crystal Growth Rates and Secondary Nucleation Threshold for γ -DL-Methionine in Aqueous Solution", J. Cryst. Growth 318(1), 117-121 (2011).
- [62] L. Wantha, and A.E. Flood, "Nucleation Kinetics of the γ-Polymorph of DL-Methionine", Chem. Eng. Technol. 35(6), 1024-1030 (2012).
- [63] L. Wantha, and A.E. Flood, "Population Balance Modeling of the Solution-Mediated Transformation of DL-Methionine Polymorphs", Chem. Eng. Technol. 36(8), 1313-1319 (2013a).
- [64] L. Wantha, A. E. Flood, "Growth and Dissolution Kinetics of α and γ Polymorphs of DL-Methionine", J. Cryst. Growth 362(1), 66-70 (2013b).
- [65] L. Wantha, and A.E. Flood, "Growth and Dissolution Kinetics of A and B Polymorphs of L-Histidine", Chem. Eng. Technol. 38(6), 1022-1028 (2015).

- [66] Z.Q. Yu, J.W. Chew, P.S. Chow, and R.B.H. Tan, "Recent Advances in Crystallization Control: An Industrial Perspectine", Chem. Eng. Res. Des. 85(7), 893-905 (2007).
- [67] L. Yu, S.M. Reutzel-Edens, and C.A. Mitchell, "Crystallization and Polymorphism of Conformationally Flexible Molecules: Problems, Patterns, and Strategies", Org. Process Res. Dev. 4(5), 396-402 (2000).
- [68] N. Zencirci, T. Gelbrich, V. Kahlenberg, and U.J. Griesser, "Crystallization of Metastable Polymorphs of Phenobarbital by Isomorphic Seeding", Cryst. Growth Des. 9(8), 3444-3456 (2009).
- [69] A.C. Zettlemoyer, Nucleation, Marcel Dekker, New York 1969.
- [70] M. Zhi, Y. Wang, J. Wang, "Determining the primary nucleation and growth mechanism of cloxacillin sodium in methanol-butyl acetate system", J. Cryst. Growth 314, 213-219 (2011).

Appendix

Output (Acknowledge the Thailand Research Fund)

Publications

- L. Wantha, and A.E. Flood, "Growth and Dissolution Kinetics of A and B Polymorphs of L-Histidine", Chem. Eng. Technol. 38(6), 1022-1028 (2015).
- L. Wantha, "Determination of Nucleation and Growth Mechanisms of the B Polymorph of L-Histidine by Induction Time Measurement", Chem. Eng. Technol. 39(7), 1289-1294 (2016).

Conference Papers

 L. Wantha, A. Laowisai, S. Pannorach, "Crystallization and Dissolution Kinetics of the Polymorphs of L-Histidine", 20th International Workshop on Industrial Crystallization (BIWIC2013), 291-296 (2013).

- 2. **L. Wantha,** A.E. Flood, "Effect of Temperature on the Growth and Dissolution Kinetics of L-Histidine", 21st International Workshop on Industrial Crystallization (BIWIC 2014), 90-96 (2014).
- L. Wantha, "Determining the Nucleation and Growth Mechanisms of B Polymorph of L-Histidine in Water-Ethanol System", 22nd International, Workshop on Industrial Crystallization (BIWIC 2015), 19-26 (2015).

Publications

Research Article Chemical Engineering
Technology

Lek Wantha¹ Adrian E. Flood²

1022

¹Burapha University, Faculty of Engineering, Department of Chemical Engineering, Chonburi, Thailand.

²Suranaree University of Technology, Institute of Engineering, School of Chemical Engineering, Nakhon Ratchasima, Thailand.

Growth and Dissolution Kinetics of A and B Polymorphs of *L*-Histidine

The growth rate of the stable polymorph A and the dissolution rate of the unstable polymorph B of L-histidine (L-his) in aqueous solution were experimentally determined at varying temperatures. The growth and dissolution kinetics were measured by means of desupersaturation and deundersaturation techniques, respectively. Both the growth and dissolution rates increase with higher temperature. At all temperatures studied, the dissolution rate of form B is faster than the growth rate of form A, indicating that the solution-mediated transformation of the polymorphs of L-his is likely to be controlled by the growth rate of form A. Both kinetics of the polymorphs of L-his will be used to characterize the polymorphic transformations and the overall crystallization rate of L-his.

Keywords: Dissolution, Growth rate, *L*-Histidine, Polymorphs, Solution-mediated transformation

Received: December 01, 2014; revised: February 11, 2015; accepted: March 13, 2015

DOI: 10.1002/ceat.201400732

1 Introduction

The essential amino acid histidine (his) is produced for a variety of products, e.g., as a food additive, an active pharmaceutical ingredient, in animal feed, and as a precursor for other chemicals. The L-histidine (L-his) crystal has previously been shown to exhibit polymorphism and it exists in the solid phase as a stable polymorph A and a metastable polymorph B [1, 2]. Form A is produced from the completed transformation of form B into form A in aqueous solution, and form B is produced from anti-solvent crystallization, where water is used as the solvent and ethanol as the anti-solvent [1, 2]. The polymorphic transformation between forms B and A is particularly significant to the processing of histidine.

Since it is necessary to prepare the appropriate polymorph for the desired application, the formation of the desired polymorph has to be controlled in polymorphic crystallization and such a process should be robust and reproducible. Usually, the formation of the polymorph is determined by thermodynamics, crystallization and dissolution kinetics, and transformation kinetics. Thermodynamics is used to identify whether the crystal phase is the stable or metastable polymorph. Kinetics enables to determine how fast these crystal phases can be crystallized at a certain driving force. Polymorphic crystallizations consist of the competitive nucleation and crystal growth of the polymorphs and the transformation from the metastable polymorph to the stable polymorph, usually via a solution-mediat-

Correspondence: Dr. Lek Wantha (lekw@eng.buu.ac.th), Burapha University, Faculty of Engineering, Department of Chemical Engineering, 169 Long-Hard Bangsaen Road, Muang District, Chonburi 20131, Thailand.

ed transformation (SMT) mechanism. This involves nucleation and crystal growth of the stable polymorph and dissolution of the metastable polymorph [3–6]. Therefore, the mechanism and kinetics of each elementary step in the crystallization process needs to be understood to predict and control the formation of the appropriate polymorph.

Accurate modeling of the SMT can be performed by creating separate models of each of the mechanisms involved and combining these models within the framework of the population balance equation (PBE) [6-8], which is a two-step method. Firstly, the rates of the crystallization processes, i.e., nucleation and growth, and the rate of dissolution of each polymorph are obtained through specific experiments. Secondly, the rates of crystallization and dissolution of each polymorph are then combined in the PBE in order to estimate the time of the transformation, polymorphic fraction profile, concentration profile, etc., which can then be compared with the results from an SMT experiment. For assistance in the characterization of the polymorphic transformation, modeling of the SMT, and overall crystallization rate of L-his, the crystallization (growth) and dissolution kinetics of each polymorph of L-his were experimentally determined in this work.

Crystal growth from solution is a two-step process [9]. The first step, namely, mass transfer by diffusion or convection, involves the transfer of molecules from the bulk solution to the crystal surface. The second step concerns the insertion of the molecules into the crystal surface, thus being a reaction step. The growth rate depends on the level of driving force for crystal growth which is the supersaturation. The dissolution process is usually considered to be controlled by the mass transfer of solute molecules from the crystal surface to the bulk, however, it may also involve a reaction step. The dissolution rate depends on the level of driving force for dissolution which is the undersaturation.

There are at least two main groups of techniques used to measure crystal growth rates. The first group involves the single-crystal growth methods, where the growth kinetics of different crystal faces are usually determined by optical or atomic force microscopy [10,11]. The second group comprises the methods considering growth in a multiparticle system [12,13]. These techniques usually measure the change in the mass or size of a group of crystals at a fixed temperature and supersaturation. When a large number of crystals are analyzed to obtain an accurate mean crystal growth rate and the extent of growth rate dispersion, the first technique may be more time-consuming than the second one.

The desupersaturation experiment is another technique which is based on measuring the change of the particle size distributions (PSDs) and solute concentrations with time in a seeded isothermal batch experiment [14–16]. The advantage of this method is that a large set of growth data can be obtained from a single experiment. The dissolution rate can be determined by the same method as the growth rate, where the size of a seed crystal, or crystals, increases with time during the growth experiment, while the size of a seed crystal, or crystals, decreases with time during the dissolution experiment [17–19].

In this work, the growth rates of form A and dissolution rates of form B of *L*-his in aqueous solution were experimentally determined. The growth and dissolution rates were measured using the desupersaturation or deundersaturation experiments in an isothermal batch crystallizer. The influence of supersaturation or undersaturation and temperature on the growth and dissolution rates was investigated. Finally, crystallization and dissolution kinetic studies have been initiated to attempt characterization of the polymorphic transformation in solution.

2 Experimental

2.1 Materials

L-his (>99 %, Sigma-Aldrich) and ethanol (>99 %, Carlo Erba Reagent) were used without further purification. All solutions were prepared with deionized water. The pure form of each polymorph was generated by the following methods. Form B crystals were crystallized by anti-solvent crystallization at room temperature as described elsewhere [1,2]. Previous studies suggested to employ mixtures of water and ethanol (>40 vol % ethanol) for producing the B-form. In this work, a saturated aqueous solution of L-his was prepared and the B-form crystallized by adding a volume of ethanol that was two times the volume of the original saturated solution. Form A crystals were obtained when the transformation from form B to form A was completed in aqueous solution at room temperature, as described elsewhere [1,2].

Pure crystal polymorphs of each form were also characterized by X-ray powder diffractometry and optical microscopy. The seed crystals of the pure form A were obtained by collecting sieved crystals in the size range of $125-250\,\mu m$. The crystal seeds of the pure form B were gained by collecting sieved crystals in the size range of $250-355\,\mu m$. The seeds of form B were prepared at a larger size since the dissolution rate experiments

involve a decrease in size of the seed crystals, which occurs relatively rapid; thus, the dissolution experiments require large seed crystals to obtain reproducible results.

2.2 Crystal Growth and Dissolution Rate Measurement

The growth rate of form A was determined via seeded batch desupersaturation experiments using time-dependent measurements of both solute concentrations and particle size distributions (PSDs) [14, 16, 19]. Experiments were performed at 10 °C, 25 °C, and 40 °C in a 0.5-L batch crystallizer (see Fig. 1) agitated by a centrally located four-blade impeller driven by an overhead stirrer at 250 rpm. The solute concentration in the clear liquor sample was measured periodically by the refractive index method, and the crystal size distribution of crystalline samples was obtained by analyzing a population of more than 30 crystals under a microscope. The growth rate was calculated as the time rate of change of the mean crystal size.

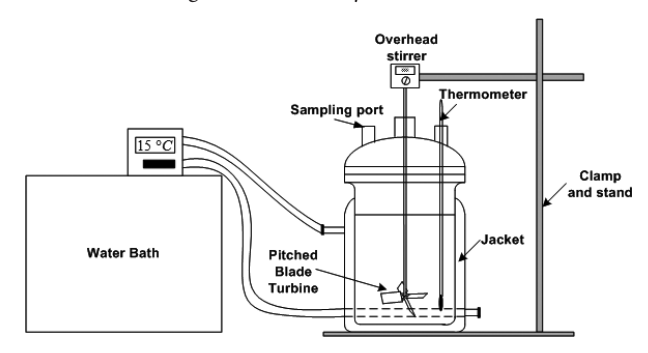


Figure 1. Crystallizer setup.

To ensure that nucleation did not occur during the experiment, the secondary nucleation thresholds were determined using a method described previously [16], and the initial supersaturation for each growth experiment was performed within the metastable region. Nucleation was not detected by the naked eye in any seeded batch crystallization for growth determination. In addition, analysis by optical microscopy did not detect any crystals smaller than the initial seed population at any time, again suggesting that nucleation did not occur during the experiment.

Desupersaturation experiments were performed in solutions that had previously been heated to 20 $^{\circ}$ C above the experimental temperature which is also at least 5 $^{\circ}$ C above the saturation temperature, for 30 to 40 min to ensure that the solution is homogeneous, and that there were no ghost nuclei remaining in the solution. The solutions were then cooled to the experimental temperature, and when the temperature reached the experimental one, a quantity of dry seeds was fed to the crystallizer. A small volume of the suspension was sampled at specific times and filtered quickly before determination of the crystal size distribution and solute concentration.

Deundersaturation experiments for determining the dissolution rates of form B were studied by a similar method to the growth experiments, except the experiments were performed at $10\,^\circ\text{C}$, $25\,^\circ\text{C}$, and $40\,^\circ\text{C}$, and under the solubility of form B.

All dry crystal samples were obtained quickly by vacuum filtration of a suspension sample by means of a membrane with 0.45 µm pore size and were washed with cold ethanol to remove water at the crystal surface. The crystal products were suspended in a saturated ethanol solution at ambient temperature, and a solution droplet was placed on a cover slip under a microscope. The population of crystals was recorded with a micrograph and the crystal size distributions were measured from the photomicrographs. The two largest visible lengths of each crystal were observed and the crystal size was calculated from the geometric mean of these two lengths. The micrographs were calibrated with a standard, and the number of crystals measured in each sample was greater than 30.

The solubility data of forms A and B in water were obtained from a previous study [1]. To analyze the repeatability of experimental results, each kinetic measurement was performed at least three times.

3 Results and Discussion

Photomicrographs of seed crystals and product crystals from a growth experiment of L-his form A at 25 °C are presented in Fig. 2. Obviously, no nucleation occurs during the growth process because no particles smaller than the seed crystals are detected. This is also confirmed by the obtained crystal size distribution (CSD). The distribution was accurate because the photos were calibrated by a standard and a large sample (> 30 crystals) was used. The shape of all crystals from the growth experiments is a rod-like which proves that the seed and product crystals are form A.

After the growth process, the concentration reaches the solubility of form A and then remains constant, as demonstrated in Fig. 3. This indicates that there was no phase transformation during the growth processes of form A.

Photomicrographs of seed crystals and product crystals from a dissolution experiment of L-his form B at 25 °C are displayed in Fig. 4. In this work, the dissolution experiments were performed for relatively short batch times to avoid the transformation process. The shape of all crystals from the dissolution experiments is plate-like, which confirms that the seed and product crystals are form B.

After the dissolution process, the concentration reaches the solubility of form B and then remains constant for some time, as shown in Fig. 5. This also proves that there was no phase transformation during dissolution of form B within the relatively short batch times of ca. 30 min. If the crystals remained in solution for an extended period, the concentration would

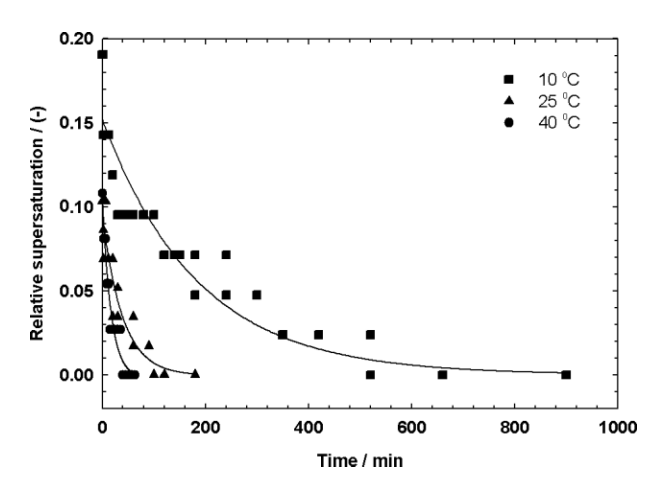


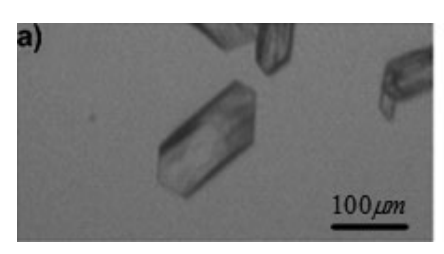
Figure 3. Desupersaturation curves from a batch run at different temperatures.

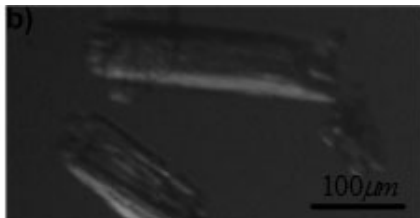
drop to the solubility of form A due to the transformation of form B into form A.

As mentioned above, Fig. 3 presents the desupersaturation curves from the growth experiments of form A. The desupersaturation rate increases with higher temperature since both the rate of mass transfer and the rate of integration of solute into the crystal surface rise with higher temperature. This indicates that the growth rate of form A increases with rising temperature as expected; see further in Fig. 8. Fig. 5 reveals that the rate of undersaturation reduction increases with higher temperature, which indicates that the dissolution rates of form B enhance with rising temperature as expected; see further in Fig. 9.

The CSDs were measured from micrographs of samples taken at particular times. The counted number of crystals for each sample was greater than 30. The number mean crystal size was determined by the total crystal length divided by the total counted number of crystals. The number mean crystal size was used to calculate the growth rate because the growth rate data can only be obtained from batch growth using the population balance, which is a number-based balance. If the volume or mass mean sizes are employed then the result is not suitable for the population balance, and therefore far less suitable.

The growth and dissolution rates can be calculated from the change of the mean crystal size divided by the change of the time of each measurement, with these being correlated to the average of the measured supersaturation at the same time. In this work, the change of mean crystal sizes with time is fitted with any continuous function that match the data well, and





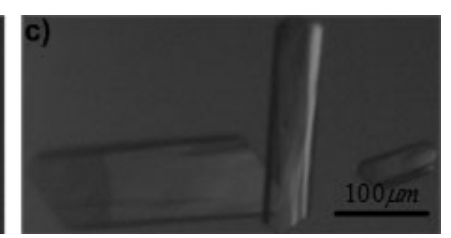
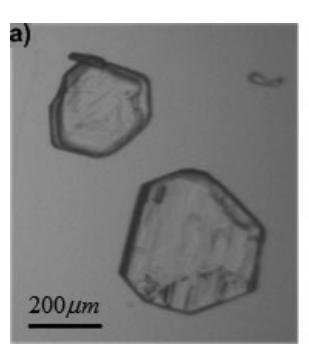
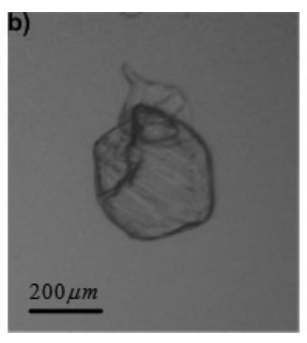


Figure 2. Photomicrographs of seed crystals and product crystals at various times from the growth experiment of form A at 25 °C: seed (a), 30 min (b), 100 min (c).





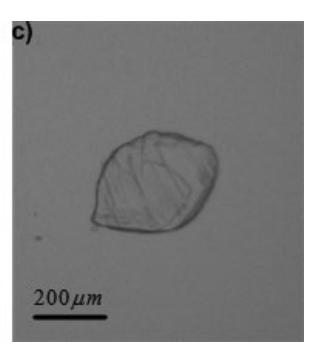


Figure 4. Photomicrographs of seed crystals and product crystals at various times from the dissolution experiment of form B at 25 °C: seed (a), 5 min (b), 13 min (c).

Numerical constants in the fitted functions were not rounded to avoid error propagation when applying further calculations to the final crystal growth rate model. An exponential rise to a maximum fits well all mean crystal sizes (µm) according to Eq. (4):

$$\overline{L} = 203 + 92(1 - e^{-0.0308t})$$
 (4)

The mean growth rate is determined as the first derivative of

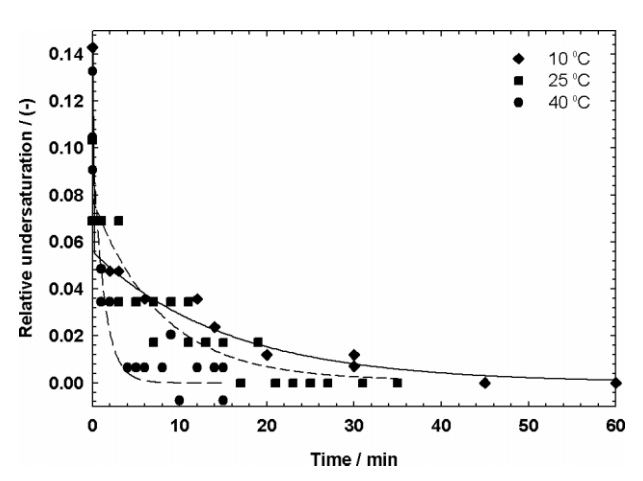


Figure 5. Deundersaturation curves from a batch run at different temperatures.

then the mean growth and dissolution rates were calculated by the following definitions:

$$\overline{G}(t) = \frac{d\overline{L}}{dt}\Big|_{t} \tag{1}$$

$$\overline{D}(t) = -\frac{\mathrm{d}\overline{L}}{\mathrm{d}t}\Big|_{t} \tag{2}$$

where $\overline{L}^{1)}$ is the mean crystal size (μ m) and t is the time (min). $\overline{G}(\sigma_G)$ and $\overline{D}(\sigma_D)$ can then be found from $\overline{G}(t)$ and $\overline{D}(t)$, respectively, using the measured concentration data as a function of time.

Fig. 6 illustrates the desupersaturation curves and time dependence of mean crystal sizes of form A for the experiments at 25 °C. An exponential decay fits very well all supersaturation data according to Eq. (3):

$$\sigma_G = 0.0960e^{-0.0258t} \tag{3}$$

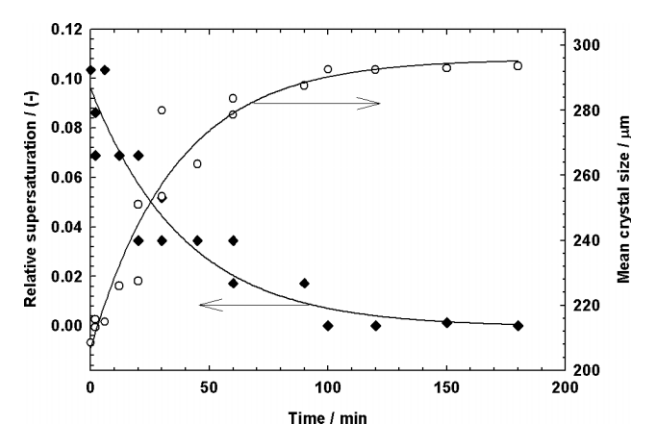


Figure 6. Desupersaturation curves and time dependence of crystal sizes of form A for the experiments at 25 °C.

mean crystal sizes (Eq. (4)) with respect to time, which is given by Eq. (5):

$$\overline{G} = \frac{d\overline{L}}{dt} = 2.832e^{-0.0308t} \tag{5}$$

The growth rates were calculated by the mean crystal size. The crystal growth experiments allowed growth rates (Eq. (5)) to be determined as a function of relative supersaturation (Eq. (3)), as shown in Fig. 8. The growth rates at 10 °C and 40 °C are determined using the same method, and the results are presented in Fig. 8. It can be seen that, at constant temperature, the growth rates increase with increasing supersaturation. This figure also indicates that the growth rates are strongly temperature dependent.

Fig. 7 displays deundersaturation curves and time dependence of crystal sizes of form B for the experiments at 25 °C. An exponential decay fits well all deundersaturation data as given by Eq. (6):

$$\sigma_D = 0.0706 e^{-0.1050t} \tag{6}$$

An exponential decay also matches well all mean crystal size data according to Eq. (7):

$$\overline{L} = 246 + 185e^{-0.1035t} \tag{7}$$

List of symbols at the end of the paper.

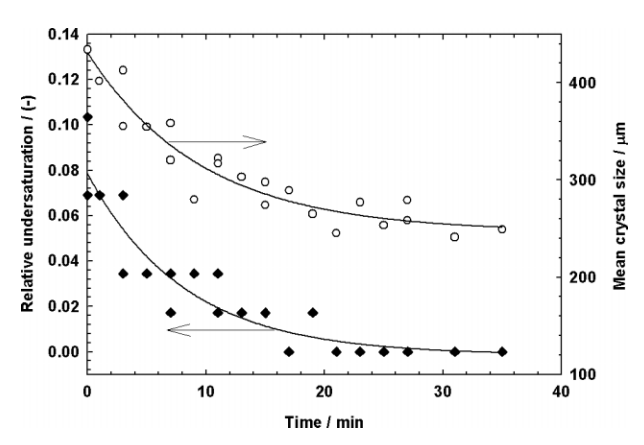


Figure 7. Deundersaturation curves and time dependence of crystal sizes of form B for the experiments at 25 °C.

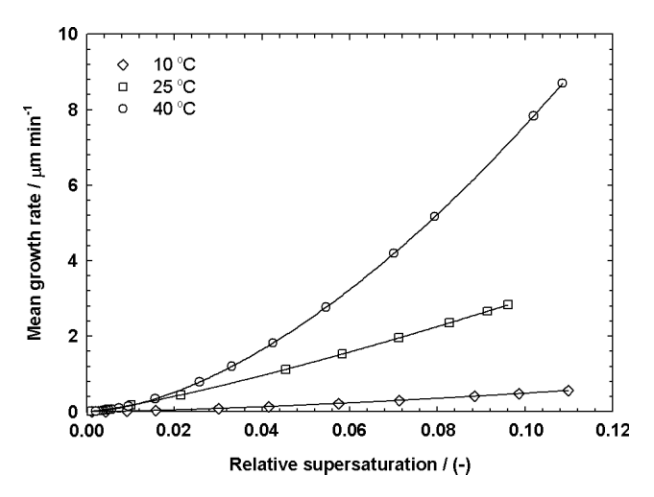


Figure 8. Mean growth rates for form A as a function of relative supersaturation.

The mean dissolution rate is determined as the first derivative of mean crystal sizes (Eq. (7)) with respect to time, which is expressed by Eq. (8):

$$\overline{D} = -\frac{d\overline{L}}{dt} = 19.11e^{-0.1035t}$$
 (8)

The dissolution rates were calculated by the mean crystal size. The dissolution experiments allowed dissolution rates (Eq. (8)) to be determined as a function of relative undersaturation (Eq. (6)), as indicated in Fig. 9. The dissolution rates at 10 °C and 40 °C are determined with the same method, and the results are shown in Fig. 9. At constant temperature, the crystal dissolution rates increase with higher undersaturation. At constant undersaturation, the dissolution rates grow with rising temperature.

The growth (or dissolution) kinetics can be expressed as a function of supersaturation (or undersaturation) for each set of conditions by the power-law model [17, 20]

$$\overline{G} = \frac{d\overline{L}}{dt} = k_G \sigma_G^n \tag{9}$$

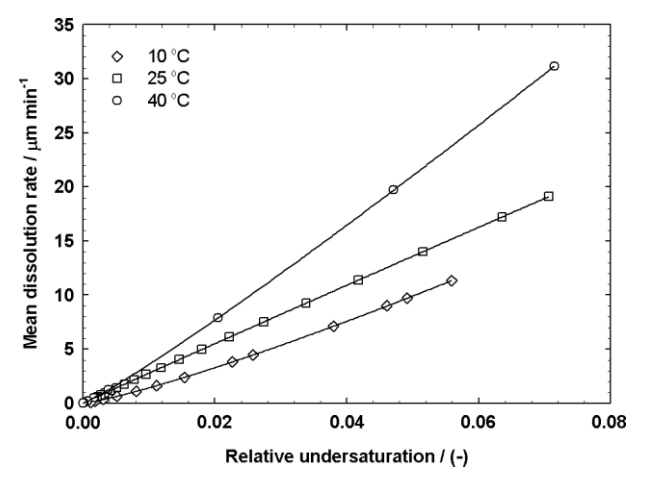


Figure 9. Mean dissolution rates for form B as a function of relative undersaturation.

$$\overline{D} = -\frac{\mathrm{d}\overline{L}}{\mathrm{d}t} = k_{\mathrm{D}}\sigma_{\mathrm{D}}^{m} \tag{10}$$

where \overline{G} and \overline{D} are the mean growth and dissolution rates ($\mu m \, min^{-1}$), respectively, $k_{\rm G}$ and $k_{\rm D}$ are the growth and dissolution rate constants ($\mu m \, min^{-1}$), $\sigma_{\rm G}$ and $\sigma_{\rm D}$ denote the relative supersaturation and undersaturation, and n and m are the growth and dissolution rate orders, respectively. The experimental results of the growth of form A and dissolution of form B were matched with Eqs. (9) and (10) using the fitting routine from the software Sigmaplot 13.0. The results are depicted in Figs. 8 and 9.

Confidence intervals of 95 % for each parameter in the model are given by the fitting routine and listed together with the parameter values in Tab. 1. The growth rate order is employed for understanding the controlling mechanism. In general, a growth rate order of n=1 indicates that mass transfer becomes a rate-controlling mechanism, and a growth rate order between 1 and 2 means that the surface integration step is at least partially rate-controlling [21]. It can be seen that in the case of the growth of form A the growth orders are 1.44 ± 0.062 , 1.23 ± 0.14 , and 1.67 ± 0.02 , respectively, for $10\,^{\circ}$ C, $25\,^{\circ}$ C, and $40\,^{\circ}$ C. This indicates that the surface integration process plays an important role in explaining the growth process of form A. For the case of the dissolution of form B, the dissolution rate orders are 1.21 ± 0.10 , 0.98 ± 0.05 , and 1.10 ± 0.23 , respectively, for $10\,^{\circ}$ C, $25\,^{\circ}$ C, and $40\,^{\circ}$ C. This signifies that at $25\,^{\circ}$ C and

Table 1. Results from kinetics parameter estimation at a 95 % confidence level.

T	Growth of from A		Dissolution of fo	orm B
	$k_{\rm G}~[\mu{\rm m~min}^{-1}]$	n [-]	$k_{\rm D} [\mu {\rm m min}^{-1}]$	m [-]
10 °C	13.64 ± 3.123	1.44 ± 0.062	366.4 ± 62.44	1.21 ± 0.10
25°C	50.69 ± 8.143	1.23 ± 0.14	260.0 ± 7.589	0.98 ± 0.05
40 °C	352.8 ± 24.09	1.67 ± 0.02	566.6 ± 139.6	1.10 ± 0.23

 $40\,^{\circ}\text{C}$ the mass transfer process plays a key role in elucidating the dissolution process of form B, and at $10\,^{\circ}\text{C}$ the surface disintegration is also important.

In crystallization of polymorphs from solution, the SMT is usually the most important process which describes the transformation from the metastable polymorph to the stable polymorph. An SMT from form B to form A will take place when crystals of form B are nucleated in or put into a saturated aqueous solution. The dissolution of form B and growth of form A are the main kinetics of SMT. As illustrated in Fig. 10, the dissolution kinetics of form B are faster than the growth kinetics of form A, i.e., the SMT of form B into form A is a growth-controlled process. This means that the mass transfer of solute from the crystal surface to the bulk solution due to the dissolution of form B rapidly proceeds to maintain the solute concentration at or close to the solubility of form B. However, the growth of form A and dissolution of form B occur simultaneously during SMT until form B crystals are completely dissolved, which signifies that the transformation is complete. Then the concentration will drop slowly to the solubility of form A due to the growth of form A. This conclusion agrees with the previous SMT study of *L*-his by Kitamura [1].

In literature, a lot of studies demonstrate that the growth of the stable polymorph is the limiting step, e.g., L-glutamic acid [22–25], taltireline [26], and carbamazepine [5,27]. The SMT of DL-methionine [6] and glycine [28] are at least two examples where the dissolution of the metastable polymorph was the limiting step.

4 Conclusions

The kinetics of growth and dissolution of the polymorphs of L-his which contribute to the rate of transformation between the polymorphs was analyzed. The growth kinetics of form A and dissolution kinetics of form B were measured at 10 °C, 25 °C, and 40 °C in an agitated batch crystallizer. The results demonstrate that both the growth and dissolution rates increase with higher temperature. The growth of form A is a sur-

face integration-controlled process and dissolution of form B is a mass transfer-controlled process except at low temperature. At all temperatures studied, the dissolution rate of form B is faster than the growth rate of form A. This indicates that the transformation is a growth-controlled process. Further crystal growth and nucleation experiments will be performed on form B, and the nucleation rate for the form A will also be measured. This should allow a complete model of the SMT to be achieved.

Acknowledgment

The authors acknowledge the financial support of the Faculty of Engineering of Burapha University, Commission on Higher Education, and Thailand Research Fund, Thailand (grant no. MRG5680123).

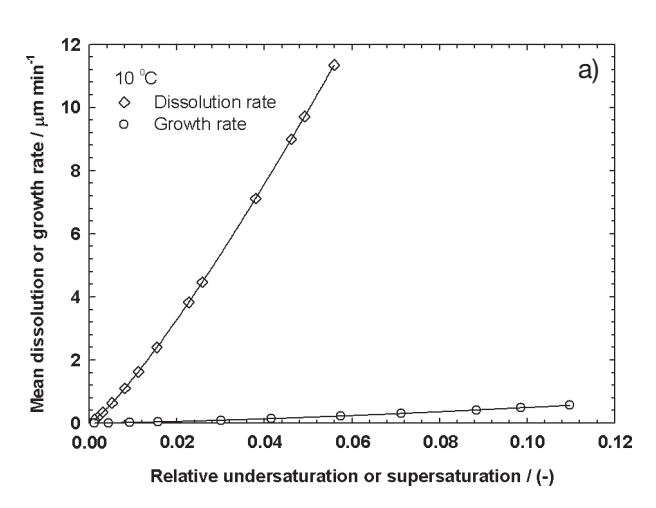
The authors have declared no conflict of interest.

Symbols used

$egin{array}{l} \overline{D} \ \overline{G} \ k_{ m D} \ k_{ m G} \ \overline{L} \ m \end{array}$	[µm min ⁻¹] [µm]	mean dissolution rate mean growth rate dissolution rate constant growth rate constant mean crystal size dissolution rate order
m n	[-]	growth rate order
t	[min]	time

Greek letters

$\sigma_{ m D}$	[-]	relative undersaturation
$\sigma_{ m G}$	[-]	relative supersaturation



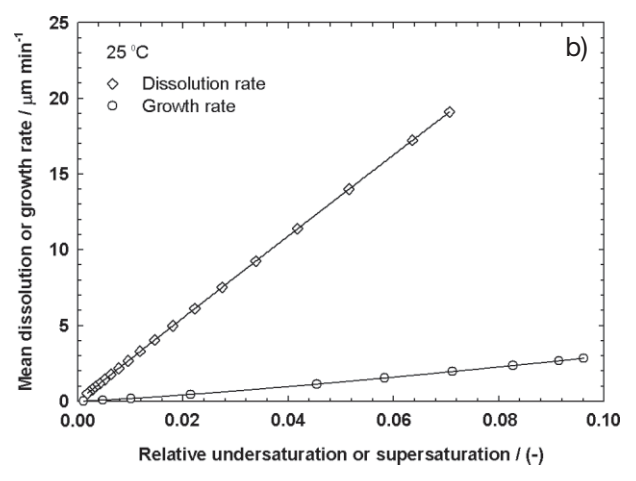


Figure 10. Mean growth rates for form A and dissolution rates for form B as a function of relative supersaturation and undersaturation at $10 \,^{\circ}$ C (a), $25 \,^{\circ}$ C (b).

References

- [1] M. Kitamura, J. Chem. Eng. Jpn. 1993, 26 (3), 303-307.
- [2] C. P. M. Roelands, S. Jiang, M. Kitamura, J. H. ter Horst, H. J. M. Kramer, P. J. Jansens, *Cryst. Growth Des.* **2006**, *6* (4), 955–963
- [3] S. Jiang, P. J. Jansens, J. H. ter Horst, Cryst. Growth Des. 2010, 10 (6), 2541–2547.
- [4] D. Mangin, F. Puel, S. Veesler, Org. Process Res. Dev. 2009, 13 (6), 1241–1253.
- [5] M. A. O'Mahony, M. Anthony, D. M. Croker, Å. C. Rasmuson, B. K. Hodnett, Cryst. Growth Des. 2012, 12 (4), 1925– 1932.
- [6] L. Wantha, A. E. Flood, Chem. Eng. Technol. 2013, 36 (8), 1313–1319.
- [7] G. Févotte, C. Alexandre, S. O. Nida, AIChE J. 2007, 53 (10), 2578–2589.
- [8] J. Scully, Ph. D. Thesis, University of Limerick 2010.
- [9] A. D. Randolph, M. A. Larson, Theory of Particulate Processes: Analysis and Techniques of Continuous Crystallization, 2nd ed., Academic Press, San Diego, CA 1988.
- [10] M. Kitamura, T. Ishizu, J. Cryst. Growth 2000, 209 (1), 138– 145
- [11] P. Pantaraks, A. E. Flood, Cryst. Growth Des. 2005, 5 (1), 365–371.
- [12] M. Kitamura, H. Furukawa, M. Asaeda, J. Cryst. Growth 1994, 141 (1-2), 193-199.
- [13] S. Srisa-nga, A. E. Flood, E. T. White, Cryst. Growth Des. 2006, 6 (3), 795–801.

- [14] J. Garside, A. Mersmann, J. Nyvlt, Measurement of Crystal Growth and Nucleation Rates, 2nd ed., Institute of Chemical Engineering, London 2002.
- [15] J. Schöll, C. Lindenberg, L. Vicum, J. Brozio, M. Mazzotti, Faraday Discuss. 2007, 136, 247–264.
- [16] L. Wantha, A. E. Flood, J. Cryst. Growth 2011, 318 (1), 117– 121.
- [17] M. Gougazeh, W. Omar, J. Ulrich, Cryst. Res. Technol. 2009, 44 (11), 1205–1210.
- [18] A. Gutjahr, H. Dabringhaus, R. Lacmann, J. Cryst. Growth 1996, 158 (3), 296–309.
- [19] L. Wantha, A. E. Flood, J. Cryst. Growth 2013, 362 (1), 66-70.
- [20] A. S. Myerson, R. Ginde, in *Handbook of Industrial Crystallization*, 2nd ed. (Ed: A. S. Myerson), Butterworth-Heinemann, Oxford 2002, 33–65.
- [21] J. W. Mullin, Crystallization, 4th ed., Butterworth-Heinemann, Oxford 2001.
- [22] S. Dharmayat, R. B. Hammond, X. Lai, C. Ma, E. Purba, K. J. Roberts, Z.-P. Chen, E. Martin, J. Morris, R. Bytheway, *Cryst. Growth Des.* 2008, 8 (7), 2205–2216.
- [23] N. Garti, H. Zour, J. Cryst. Growth 1997, 172 (3-4), 486-498.
- [24] T. Ono, H. J. M. Kramer, J. H. ter Horst, P. J. Jansens, Cryst. Growth Des. 2004, 4 (6), 1161–1167.
- [25] J. Schöll, D. Bonalumi, L. Vicum, M. Mazzotti, Cryst. Growth Des. 2006, 6 (4), 881–891.
- [26] S. Maruyama, H. Ooshima, J. Kato, Chem. Eng. J. 1999, 75 (3), 193–200.
- [27] H. Qu, M. Louhi-Kultanen, J. Rantanen, J. Kallas, Cryst. Growth Des. 2006, 6 (9), 2053–2060.
- [28] E. S. Ferrari, R. J. Davey, W. I. Cross, A. L. Gillon, C. S. Towler, Cryst. Growth Des. 2003, 3 (1), 53.

Lek Wantha

Department of Chemical Engineering, Faculty of Engineering, Burapha University, Chonburi, Thailand.

Determination of Nucleation and Growth Mechanisms of the B Polymorph of L-Histidine by Induction Time Measurement

The nucleation and growth mechanisms of the B polymorph of L-histidine (L-his) in a water-ethanol system were determined based on induction time measurements. The induction times were experimentally determined at different supersaturations and correlated using the models of mononuclear and polynuclear mechanisms. The primary nucleation mechanism of the B polymorph of L-his was identified as a polynuclear mechanism and the growth mechanism was found to be a two-dimensional nucleation-mediated growth. These mechanisms of the B polymorph of L-his will be used to characterize the polymorphic transformations and the overall crystallization rate of L-his.

Keywords: B polymorph of *L*-histidine, Growth mechanism, Nucleation mechanism, Polymorphic transformation

Received: January 17, 2016; revised: April 10, 2016; accepted: May 09, 2016

DOI: 10.1002/ceat.201600045

1 Introduction

In crystallization from a solution of a polymorphic compound when a driving force is imposed, the system tends to minimize its free energy. This leads to the crystallization of the most stable polymorph. However, the system may crystallize into the less stable polymorph first if its crystallization kinetics is faster, and then the less stable polymorph may transform into the more stable one [1]. This phenomenon of formation of the kinetically controlled polymorph over the thermodynamically favored form is known as Ostwald's rule of stages [2]. Moreover, if both polymorphs crystallize at similar rates, a mixture of the two polymorphs is initially obtained which is called concomitant polymorphism [3].

In the case of Ostwald's rule, there are two different steps that can be identified as fundamental mechanisms governing the transformation process [4]. The first step is the nucleation and growth of the metastable polymorph. The second step is the solution-mediated transformation (SMT), which consists of the nucleation and crystal growth of the stable polymorph and the dissolution of the metastable polymorph.

To control polymorph formation, the mechanism of each elementary step in the crystallization process needs to be understood. Accurate kinetic information allows process modeling and enables process design, optimization, and control. Therefore, the determination of crystallization, i.e., nucleation

Correspondence: Dr. Lek Wantha (lekw@eng.buu.ac.th), Department of Chemical Engineering, Faculty of Engineering, Burapha University, 169 Long-Hard Bangsaen Road, Muang District, Chonburi 20131, Thailand.

and growth, and the dissolution mechanism are important for characterizing the crystallization behavior and transformation of the polymorphs.

In this study, the nucleation and growth mechanisms of the B polymorph of L-histidine (L-his) in a water-ethanol system are described. L-His, an essential amino acid, is of great importance in food, pharmaceutical, and feed industries and serves as a precursor for other chemicals. There are two known polymorphic forms of L-his crystals: a stable polymorph A and a metastable polymorph B [5,6]. A mixture of forms A and B results from cooling crystallization of L-his in aqueous solution. Then the pure form A is generated from the completed transformation of form B into A. Form B is produced from anti-solvent crystallization whose volume fraction of the anti-solvent is greater than 0.4, where water is used as the solvent and ethanol as the anti-solvent. The polymorphic transformation between these two forms is particularly significant to the processing of histidine.

The determination of the nucleation and growth rates is of key importance for the development of process models that can be used for process design and optimization, including models of the SMT. Up to now, numerous techniques for determination of the nucleation are available, and growth rates for the crystallization process have been proposed in the literature, e.g., methods using combined particle (crystal) counting and process time measurements [7,8], mixed-suspension mixed-product removal (MSMPR) experiments in combination with particle size distribution (PSD) measurements [9,10], induction time measurements [11–13], and metastable zone experiments [14,15]. The most commonly applied method is induction time measurement [11–13]. In [12,13], theoretical expressions have been used to prove the dependence of the induction time on the supersaturation for different crystal

growth mechanisms. These expressions have been shown to be correct in identifying the nucleation and growth mechanisms.

In this study, the nucleation and growth mechanisms of the B polymorph of L-his in a water-ethanol solution were determined by induction time measurements. The induction times were assessed in an isothermal batch crystallizer at different supersaturations and 25 °C. The influence of supersaturation on the induction times was investigated. Finally, the experimental results of induction time were correlated by the models of mononuclear and polynuclear mechanisms to identify the nucleation and growth mechanisms.

2 Theory

The classical nucleation theory (CNT) of primary nucleation has been described as follows by Kuldipkumar et al. [16]. The rate of primary nucleation can be defined according to the following equation:

$$J = A \exp\left(\frac{-4f_s^3 \gamma^3 \nu^2}{27f_v^2 \kappa^3 T^3 (\ln S)^2}\right)$$
 (1)

where $A^{1)}$ is the pre-exponential factor, γ is the interfacial free energy between crystal and solution, ν is the molecular volume of the crystal, κ is the Boltzmann constant, T is the absolute temperature, S is the supersaturation, f_s is the surface shape factor, and f_v is the volume shape factor.

For a mononuclear nucleation mechanism, Mullin [17] suggested that the induction time period $t_{\rm ind}$ is inversely proportional to the nucleation rate ($t_{\rm ind}=1/JV$). Therefore, Eq. (1) can be rewritten as:

$$\ln(t_{\rm ind}) = A_{\rm m} + \frac{B}{(\ln S)^2} \tag{2}$$

when

$$A_{\rm m} = \ln \frac{1}{AV} \tag{3}$$

$$B = \frac{4f_s^3 \gamma^3 \nu^2}{27f_v^2 \kappa^3 T^3} \tag{4}$$

where V is the volume of the system. Plotting of $\ln(t_{\rm ind})$ against $1/(\ln S)^2$ results in a straight line of slope B, and intercept of axis y of $A_{\rm m}$. The different slopes suggest that the homogeneous (at high supersaturation) and heterogeneous (at low supersaturation) nucleation mechanisms may exist [17].

Eq. (2) is valid when the induction time is dominated by the time required for the critical nuclei formation, i.e., the nucleation is due to a mononuclear nucleation mechanism [13]. However, Eq. (2) will be invalid if the induction time is dominated by the time required to grow the nucleus to a detectable size [13]. Therefore, the polynuclear mechanism should be adopted to characterize the nucleation.

The induction time for the formation of a new phase by the polynuclear mechanism is usually expressed as [16]:

$$t_{\text{ind}} = \left[\frac{\alpha}{a_n I G^{n-1}} \right]^{1/n} \tag{5}$$

where α is the volume fraction of the detected new phase, G is the growth rate of nucleus, a_n is the shape factor, and n=mb+1, where m refers to the dimensionality of growth, and b=0.5 or 1 denotes that the crystal growth is controlled by volume diffusion or by surface integration process, respectively. Because the B polymorph of L-his is a plate crystal [5], a 2D growth (m=2) can be assumed. Because the growth of the L-his crystal is controlled by surface integration process [18], b=1.

For the polynuclear nucleation mechanism, the pre-exponential factor in Eq. (1) depends on the supersaturation [19]. Therefore, the steady-state nucleation rate is written as:

$$J = K_J \operatorname{Sexp}\left(\frac{-B}{(\ln S)^2}\right) \tag{6}$$

where K_I is the nucleation rate constant.

The general growth kinetics can be expressed as a function of supersaturation by the power-law model [10, 17]:

$$G = K_G (S-1)^g \tag{7}$$

where $K_{\rm G}$ is the growth rate constant, and g is the growth rate order and indicates the growth mechanism. In general, a growth rate order of g=1 indicates that mass transfer becomes a rate-controlling mechanism, and a growth rate order between 1 and 2 signifies that the surface integration step is rate-controlling and represents the "birth and spread" growth mechanism, while g>2 represents a spiral growth mechanism. Inserting Eqs. (6) and (7) into Eq. (5) and taking the logarithm of the induction time (with m=2 and b=1), the following relationship is obtained:

$$\ln(t_{\text{ind}}) = \ln A_{\text{p}} - \frac{2g}{3} \ln(S - 1) - \frac{1}{3} \ln S + \frac{B}{3(\ln S)^2}$$
 (8)

when

$$A_{\rm p} = \left(\frac{\alpha}{a_n K_I K_G^2}\right)^{1/3} \tag{9}$$

The parameters A_p , B, and g can be determined by correlating the induction time with the supersaturation. The nucleation and growth mechanisms can be identified by comparing the coefficient of determination R^2 or values of g (Eq. (8)).

3 Experimental

3.1 Materials

Pure *L*-his powder (>99%, Sigma-Aldrich), and ethanol (>99%, Carlo Erba Reagent) were used without further purification. Deionized water was used in all experiments.

¹⁾ List of symbols at the end of the paper.

3.2 Induction Time Measurement

Nucleation mechanisms were determined by induction time measurement. These measurements of L-his in water-ethanol solution were performed at 25 °C in a 0.25-L batch crystallizer (Fig. 1). A series of saturated solution (aqueous solution of L-his) was prepared and heated to 5 °C above saturation temperature for 30–40 min to ensure that no ghost nuclei remained in the solution. Then the solution was cooled to experimental temperature and kept at this level. When the experimental temperature was reached, ethanol was added to the solution. The induction time was then measured by recording the appearance of the crystals by eye. Three reproducible experiments were carried out for the different supersaturation levels tested.

4 Results and Discussion

From a previous study [6], pure-form B crystals were crystallized by anti-solvent crystallization. It was suggested that the fraction of ethanol added to the saturated solution (L-his in water) should be greater than 0.4 by volume. Therefore, in this study, the fraction of ethanol added started at 0.5. Fig. 2 presents the photomicrographs of crystals obtained from the completed transformation of form B into A in aqueous solution at 25 °C (Fig. 2 a) compared with crystals obtained from the

water-ethanol system at 25 °C (Fig. 2 b). Fig. 2 a demonstrates that the shapes of all crystals obtained is rod-like, which indicates that the product crystals are form A. According to Fig. 2 b, the shape of all crystals obtained from crystallization at 50 vol % ethanol is plate-like, which points to form B of the product crystals.

Pure crystal polymorphs of each form were characterized by X-ray powder diffraction (XRPD) as displayed in Fig. 3. All crystals obtained in this study were also characterized by microscopy and XRPD.

The induction times of the B polymorph of L-his in the water-ethanol solution are given in Fig. 4. Each point represents the mean of experimental data from at least three measurements. It can be observed that the induction time decreases with increasing supersaturation ratio. The numbers in the bracket represent the volume fraction of ethanol added to the solution. It is obvious that the induction time becomes shorter with higher fraction of ethanol. It can be concluded that the nucleation rate of L-his increases with higher supersaturation ratio and fraction of ethanol. The nucleation kinetics of the metastable form B is one of the important parameters for characterization of the polymorphic transformation of *L*-his.

A plot of $ln(t_{ind})$ against $1/(lnS)^2$ of the nucleation experiments of the B polymorph

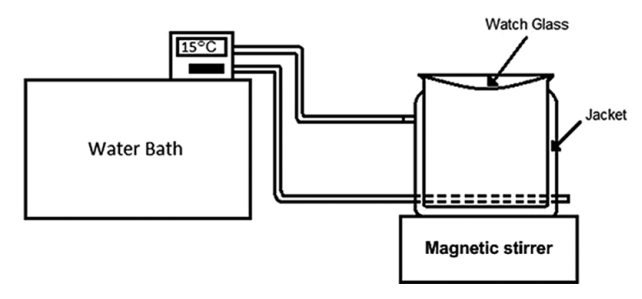
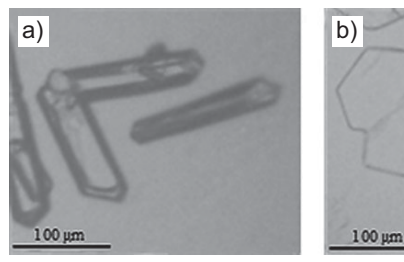


Figure 1. Crystallizer setup.



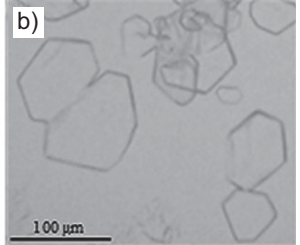


Figure 2. Photomicrographs of product crystals: (a) obtained from the completed transformation of form B into form A in aqueous solution at $25\,^{\circ}$ C, (b) from water-ethanol system at $25\,^{\circ}$ C, $50\,\text{vol}$ % ethanol.

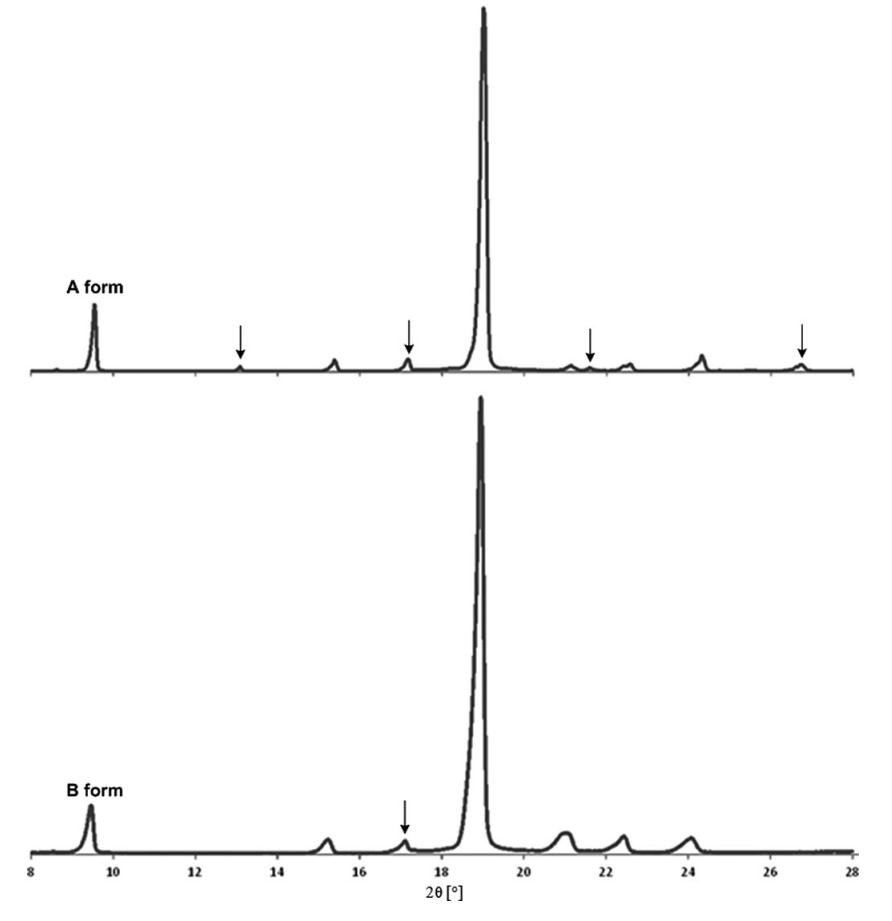


Figure 3. X-ray powder diffraction patterns of forms A and B.

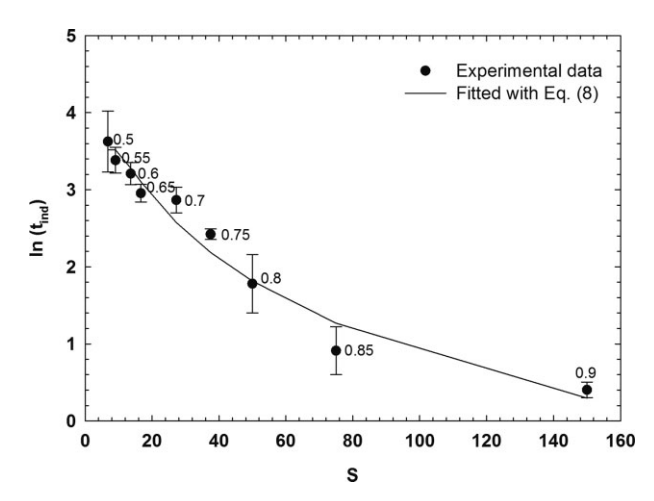


Figure 4. Measured induction times as a function of supersaturation ratio for different volume fractions of ethanol added at 25 °C.

of *L*-his in aqueous-ethanol solution at 25 °C is illustrated in Fig. 5. The fitted line with Eq. (2) is not satisfying ($R^2 = 0.6747$). However, Mullin [17] suggested that the line would be separated into two straight lines corresponding to the mechanisms of homogeneous and heterogeneous nucleation. The corresponding plot is given in Fig. 6. This result is similar those of other investigations reported previously [13, 20].

These two lines are separated based on the system nucleating at low and high supersaturations. The shorter induction time was recorded as supersaturation increases. This is probably because a higher solution supersaturation effectively reduces the size of a critical nucleus, and hence, shortens the induction time. Moreover, the results demonstrate that at a higher solution concentration, the onset of crystallization occurs at a shorter induction period. A greater supply of fresh solution at higher solution concentrations results in a prolonged lifetime of nuclei which then enhances the crystal growth.

The measured nucleation kinetics follows the trends expected from the CNT. The best-fit values of $A_{\rm m}$ and B are listed

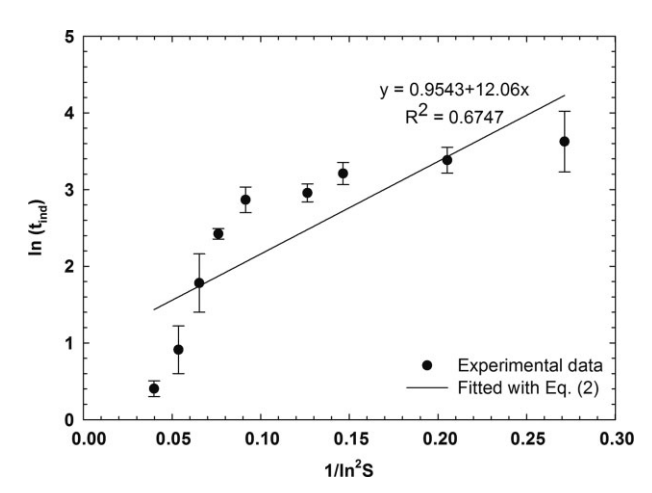


Figure 5. Dependence of induction time on supersaturation ratio of the B polymorph of L-his in water-ethanol solution at 25 °C. Data are fitted using Eq. (2).

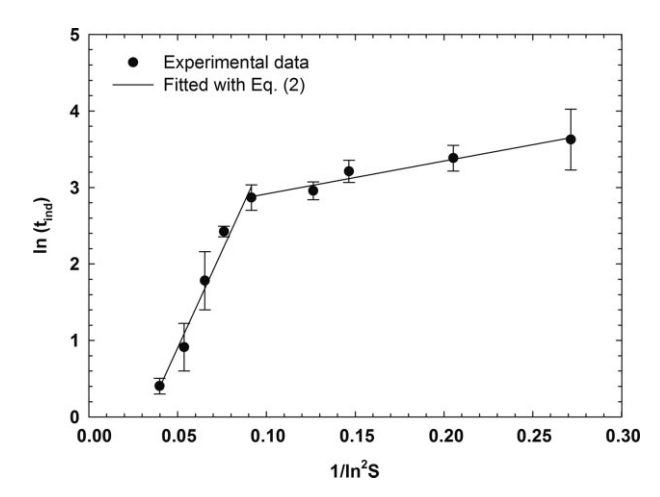


Figure 6. Dependence of induction time on supersaturation ratio of the B polymorph of L-his in water-ethanol solution at 25 °C. Data are fitted using Eq. (2). The fitted line is separated into two straight lines.

in Tab. 1. As indicated in this table (mononuclear mechanism), the lowest coefficient of determinations \mathbb{R}^2 is 0.96. This means that the correlation between the induction time and Eq. (2) is not very good.

Table 1. Parameters and coefficient of determination in Eq. (2).

Nucleation	$A_{ m m}$	В	R^2
Homogeneous	-1.636	50.75	0.9763
Heterogeneous	2.488	4.285	0.9603

In comparison with the polynuclear mechanism, it is necessary to correlate the induction time with Eq. (8). Parameters and the coefficient of determinations in Eq. (8) are listed in Tab. 2. A plot of $\ln(t_{\rm ind})$ against $1/(\ln S)^2$ and data fitted using Eq. (8) are displayed in Fig. 7.

According to Tab. 2, the coefficient of determination R^2 is above 0.99 which means an excellent correlation between the induction time and Eq. (8). This indicates that the nucleation mechanism of the B polymorph of L-his in the water-ethanol system at 25 °C is governed by the polynuclear mechanism, where the metastability is lost by nucleation and growth of nuclei. Moreover, g=1.81 signifies that the growth of the B polymorph of L-his in the water-ethanol system at 25 °C is a "birth and spread" growth mechanism, which belongs to the 2D nucleation-mediated growth [21].

Table 2. Parameters and coefficient of determination in Eq. (8).

Parameter	Value	
lnA_p	8.299	
В	-22.28	
g	1.810	
R^2	0.9926	

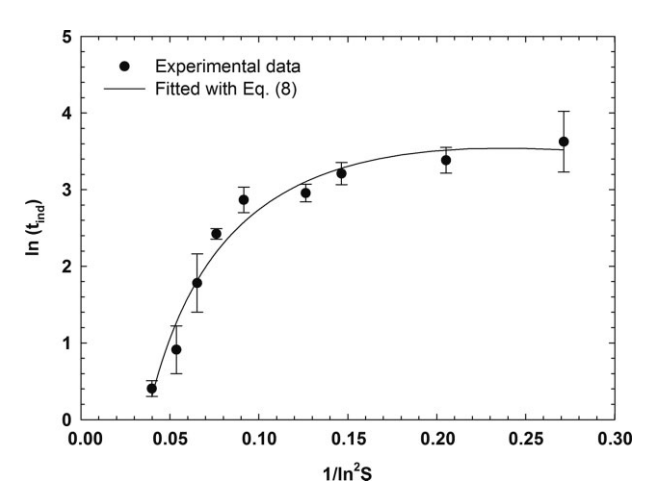


Figure 7. Dependence of induction time on supersaturation ratio of the B polymorph of L-his in water-ethanol solution at 25 °C. Data are fitted using Eq. (8).

5 Conclusions

The mechanisms of nucleation and growth of the B polymorph of L-his in water-ethanol solutions were determined and evaluated by induction time measurements. The experimental data can be separated into two straight lines corresponding to the mechanisms of homogeneous and heterogeneous nucleation. Induction time increases with decreasing supersaturation and ethanol fraction. Nucleation is governed by a polynuclear mechanism. The growth mechanism reveals a 2D nucleation-mediated growth. A further nucleation mechanism for form A will also be determined. This should allow for achieving a complete model of solution-mediated transformation.

Acknowledgment

The author gratefully acknowledges the financial support of the Faculty of Engineering of Burapha University, Commission on Higher Education, and Thailand Research Fund, Thailand, and the XRPD support by the Frontier Research Center, Vidyasirimedhi Institute of Science and Technology, Thailand. The author is also grateful to N. Punmalee and V. Sawaddiphol for their help in taking microscope images.

The author has declared no conflict of interest.

Symbols used

a_n	[-]	shape factor
A	$[m^{-3}s^{-1}]$	pre-exponential factor
A_{m}	[-]	pre-exponential factor for mononuclear
		nucleation mechanism

A_{p}	[-]	pre-exponential factor for polynuclear
-		nucleation mechanism
$f_{\rm s}$	[-]	surface shape factor
$f_{\rm v}$	[-]	volume shape factor
g	[-]	growth rate order
G	$[m s^{-1}]$	growth rate
J	$[m^{-3}s^{-1}]$	nucleation rate
$K_{\rm G}$	$[m s^{-1}]$	growth rate constant
K_I	$[m^{-3}s^{-1}]$	nucleation rate constant
m	[-]	dimensionality of growth
S	[-]	supersaturation
$t_{\rm ind}$	[s]	induction time
T	[K]	absolute temperature
V	$[m^3]$	volume of the system
		•

Greek letters

α	[-]	volume fraction of the detected new
		phase
γ	$[J m^{-2}]$	interfacial free energy between crystal and
		solution
κ	$[J K^{-1}]$	Boltzmann constant
ν	$[m^3]$	molecular volume of the crystal

References

- C. P. M. Roelands, *Ph.D. Thesis*, Delft University of Technology 2005.
- [2] T. Threlfall, Org. Process Res. Dev. 2003, 7 (6), 1017–1027.
- [3] J. Bernstein, R. J. Davey, J. O. Henck, Angew. Chem., Int. Ed. 1999, 38 (23), 3440–3461.
- [4] S. Jiang, P. J. Jansens, J. H. ter Horst, Cryst. Growth Des. 2010, 10 (6), 2541–2547.
- [5] M. Kitamura, J. Chem. Eng. Jpn. 1993, 26 (3), 303-307.
- [6] C. P. M. Roelands, S. Jiang, M. Kitamura, J. H. ter Horst, J. W. M. Kramer, J. P. Jansens, *Cryst. Growth Des.* 2006, 6 (4), 955–963.
- [7] C. Lindenberg, M. Mazzotti, AIChE J. 2011, 57 (4), 942–950.
- [8] L. Wantha, A. E. Flood, Chem. Eng. Technol. 2012, 35 (6), 1024–1030
- [9] J. Garside, A. Mersmann, J. Nyvlt, Measurement of Crystal Growth and Nucleation Rates, 2nd ed., Institution of Chemical Engineers, Rugby 2002.
- [10] Crystallization Technology Handbook, 2nd ed. (Ed: A. Mersmann), Marcel Dekker, New York 2001.
- [11] C. Lindenberg, M. Mazzotti, J. Cryst. Growth 2009, 311 (4), 1178–1184.
- [12] S. Teychené, B. Biscans, Cryst. Growth Des. 2008, 8 (4), 1133–1139.
- [13] M. Zhi, Y. Wang, J. Wang, J. Cryst. Growth 2011, 314 (1), 213–219.
- [14] Z. K. Nagy, M. Fujiwara, X. Y. Woo, R. D. Braatz, Ind. Eng. Chem. Res. 2008, 47 (4), 1245–1252.
- [15] N. A. Mitchell, P. J. Frawley, J. Cryst. Growth 2010, 312 (19), 2740–2746.
- [16] A. Kuldipkumar, G. S. Kwon, G. G. Zhang, Cryst. Growth Des. 2007, 7 (2), 234–242.

- [17] J. W. Mullin, Crystallization, 4th ed., Butterworth-Heinemann, Oxford 2001.
- [18] L. Wantha, A. E. Flood, Chem. Eng. Technol. 2015, 38 (6), 1022–1028.
- [19] Nucleation (Ed: A. C. Zettlemoyer), Marcel Dekker, New York 1969.
- [20] J. Schöll, L. Vicum, M. Müller, M. Mazzotti, Chem. Eng. Technol. 2006, 29 (2), 257–264.
- [21] *Handbook of Industrial Crystallization*, 2nd ed. (Ed: A. S. Myerson), Butterworth-Heinemann, Woburn, MA **2001**.